Quantification of the Propeller Slipstream Effect on Ice Shed Trajectories

by

Bilal Yassine

THESIS PRESENTED TO ÉCOLE DE TECHNOLOGIE SUPÉRIEURE
IN PARTIAL FULFILLMENT OF A MASTER'S DEGREE
WITH THESIS IN AEROSPACE ENGINEERING
M.A.Sc.

MONTREAL, APRIL 05, 2022

ÉCOLE DE TECHNOLOGIE SUPÉRIEURE
UNIVERSITÉ DU QUÉBEC

BOARD OF EXAMINERS

THIS THESIS HAS BEEN EVALUATED

BY THE FOLLOWING BOARD OF EXAMINERS

Mr. François Morency, Thesis supervisor
Department of Mechanical Engineering, École de Technologie Supérieure

Mr. Stéphane Hallé, Chair, Board of Examiners
Department of Mechanical Engineering, École de Technologie Supérieure

Mrs. Marlène Sanjosé, Member of the Jury
Department of Mechanical Engineering, École de Technologie Supérieure

THIS THESIS WAS PRESENTED AND DEFENDED

IN THE PRESENCE OF A BOARD OF EXAMINERS AND THE PUBLIC

ON FEBRUARY 22, 2022

AT ÉCOLE DE TECHNOLOGIE SUPÉRIEURE

ACKNOWLEDGEMENTS

My time at École de technologie supérieure (ÉTS) was memorable and I am happy to be able to use this space to thank all those who have participated directly or indirectly in making the realization of this master thesis. I realize that my long journey of becoming an aerospace engineer is almost ending. Reaching the end of this was impossible without my supervisor François Morency professional guidance and feedback on my work. His dynamism and continuous encouragement helped me to lead this work well.

My thanks also go to the members of the jury who do me the honour of evaluating this master thesis.

Also, I would like to give huge thanks to Hassan El Sahely for all the help and motivation to achieve this work. This one goes to Vincent Malenfer, for being my best roommate and for his help to stay motivated during the Covid-19. Thank you for reminding me of the right decision and make me see the best solution in me in my stressful moments

Special thanks to Kevin, Mohamed, Sébastien, Aida, Momchil, Ayman and Rasoul for their moral support and advise love, patience and encouragement.

Many thanks to my friends and colleagues from ÉTS (office:2360) who have helped generate a stimulating work environment. A master's degree is not always a part of pleasure, without their joy and good humour, my time in Montréal would not have been the same.

Finally, I particularly want to thank my father Doctor Zouheir Yassine for all his emotional and financial support to pursue my dream. And as you told me, 'You can and you will be an aerospace engineer.' My mother Majeda Majzoub who was always encouraging me to be strong in this journey.

I mainly dedicate this work to my parents who always give me the desire to go further and surpass myself in life. They were able to encourage me these months to complete this thesis and, I am proud to be able to dedicate this work to them.

As well, I dedicate this work to my lovely wife Yuliia Yassine for her love, her patience. I am so happy that you are next to me at the end of this journey and sharing the happiness of the successful future coming. Your support and efforts during my studies throughout this project.

VI

The beginning of 2022 brought me two joys your presence next to me and our lovely child. I love you to the moon and back.

Quantification de L'effet du Sillage d'une Hélice sur la Trajectoire des Particules de Glace Détachées

Bilal Yassine

RÉSUMÉ

L'accumulation de glace est un risque naturel important qui peut se produire pendant le vol. Elle peut entraîner une dégradation des performances aérodynamiques de l'avion. Les particules de glace détachées de l'aile frappent et endommagent les composants de l'avion à l'impact. Leurs trajectoires inconnues réduisent la sécurité des structures de l'avion, entraînant des réparations importantes et des accidents graves. Des études numériques de ces trajectoires inconnues sont employées afin de réduire ces dangers. Une bonne façon de représenter la probabilité qu'une particule traverse un plan perpendiculaire au fuselage est appelée carte d'empreintes. L'objectif de cette thèse est de construire un outil capable d'étudier la carte d'empreintes des trajectoires de glace derrière l'hélice et l'aile. Une méthode de panneaux 3D (3DPM) est utilisée comme approche numérique pour calculer le champ d'écoulement et ces trajectoires inconnues autour de l'hélice et de l'aile. En outre, un outil numérique appelé Qprop advanced Blade element method (théorie avancée du momentum des éléments de pale ou BEMT) est utilisé. Qprop est utilisé pour déterminer les vitesses induites nécessaires pour représenter le courant induit par l'hélice. La combinaison de 3DPM et de BEMT est utilisée comme un outil numérique rapide pour réaliser l'étude de l'interaction entre l'hélice et l'aile. Une étude paramétrique est réalisée sur la base d'un cas test sur une seule trajectoire de glace afin de montrer les effets des paramètres sur la trajectoire de glace. De plus, une étude probabiliste des empreintes des particules de glace est faite sur la base de 1000 trajectoires pour observer la zone la plus touchée par les morceaux de glace. Aussi, la Fonction de Distribution de Probabilité (Probability Distribution Function ou PDF) du souffle de l'hélice est comparée à la PDF de la littérature connue de la zone de l'aile sans glissement d'hélice. Cette comparaison permettra de mieux comprendre la menace permanente que représente le souffle de l'hélice pour la sécurité aérienne. Cela peut être utile sur différentes configurations d'hélice et d'aile pour étudier les trajectoires de la glace autour des avions.

Cette étude a permis de tirer trois conclusions principales. Premièrement, les trajectoires de glace ont été significativement affectées par le souffle de l'hélice, comme le montre l'étude paramétrique (trajectoire de glace unique). Ceci a été confirmé par la quantification de l'effet du glissement de l'hélice sur l'avion sur 1000 trajectoires blocs de glace. Une portance plus faible et un taux d'accrétion plus élevé au-dessus de l'aile derrière l'hélice ont été observés. Par conséquent, les modèles basés uniquement sur les ailes manquent un élément clé : pour les avions à turbopropulseurs, le souffle de l'hélice doit être pris en compte. La deuxième constatation est la validation de la chute du coefficient de pression sur l'aile derrière l'hélice. Enfin, la troisième constatation est l'impact potentiel de la glace sur le fuselage lors de la diminution de la vitesse de courant induit.

Mots-clés: Accrétion de glace, carte d'empreintes, BEMT, 3DPM, QProp, PDF

Quantification of the Propeller Slipstream Effect on Ice Shed Trajectories

Bilal Yassine

ABSTRACT

Ice accretion is a significant natural hazard which can occur during flight. It can lead to the degradation of the aircraft aerodynamic performance. For decades, engineers have tried to solve this ice accretion problem by integrating de-icing and anti-icing devices on the aircraft frame to maintain the performance. Nevertheless, the unknown trajectories of the detached particles remained an issue due to the complex physical flows around the aircraft. The detached ice particles from the wing or propeller strike the aircraft components, damaging them on impact. Their unknown trajectories reduce the safety of the aircraft structures, leading to major repairs and severe accidents. Numerical studies of these unknown trajectories are employed in order to reduce these dangers, especially behind the engine propeller where the ice particles are dismantled with high velocity. A good way of representing the probability of a trajectory to cross a plane perpendicular to the fuselage is called a footprint map. The objective of this thesis is to build a tool capable of studying the ice trajectory footprint map behind the propeller and the wing geometries. To correctly predict a footprint map at the propeller section of a turboprop, a 3D panel method (3DPM) is used as the numerical approach to compute the flowfield and these unknown trajectories around the propeller and wing. Additionally, a numerical tool called (Qprop) advanced Blade Element Method (BEMT) is used. (Qprop) is employed to determine the induced velocities needed to represent the slipstream produced by the propeller. The combination of both 3DPM and BEMT is used as a numerical tool for performing the interaction between propeller and wing study. A parametric study is made based on test cases on a single ice trajectory to show the parameters' effect on the ice trajectory. Also, a probabilistic study of the ice particles footprints is done based on the 1000 trajectories to observe the most hit area by the ice chunks. Moreover, the Probability Distribution Function (PDF) in the area of the slipstream of the propeller is compared with the known literature PDF wing area without propeller slipstream. This comparison will allow for a better understanding of the ongoing threat to aviation safety of the propeller slipstream. This can be useful on different propeller and wing configurations to study the ice shed trajectories on various aircraft.

Three main findings were yielded from this study. First, the ice trajectories were significantly affected by the propeller slipstream, as seen through the parametric study (single ice trajectory). This was supported further by the quantification of the propeller slipstream on the aircraft on 1000 ice trajectories. A lower lift and a higher rate of accretion above the wing behind the propeller were observed. Therefore, wing-only models are missing a key element : for turbo-prop aircraft, the propeller slipstream must be taken into account. The second finding is the validation of the drop in pressure coefficient on the wing behind the propeller. Finally, the third finding is the potential ice impact on the fuselage when decreasing the slipstream induced velocity.

Keywords: Ice accretion, footprint map, BEMT, 3DPM, QProp, PDF

TABLE OF CONTENTS

Page

LIST OF TABLES

LIST OF FIGURES

LIST OF ABBREVIATIONS

2D	Two-dimensional
3D	Three-dimensional
AOA	Angle Of Attack
AR	Aspect ratio
BEM	Blade Element Momentum
BEMT	Blade Element Momentum Theory
BWB	Blended Wing Body
CFD	Computation Fluid Dynamics
CG	Center of gravity
CP	Centre of pressure
FAA	Federal Aviation Administration
FAR	Federal Airworthiness Regulation
MATLAB	MATrix LABoratory
NACA	National Advisory Committee for Aeronautics
NASA	National Aviation and Space Administration
PDF	Probability Distribution Function
PM	Panel Method
RANS	Reynold Averaged Navier-Stokes
RHS	Right Hand Side

RPM	Revolutions Per Minute
SBA	Sweepback angle
SR	Surface Ratio
UAV	Unmanned Aerial Vehicle
VLM	Vortex Lattice Method

LIST OF SYMBOLS AND UNITS OF MEASUREMENTS

Φ	Potential flow velocity
C_p	Pressure coefficient
v_a	Axial induced velocity at disc
v_t	Tangential induced velocity at disc
v_e	Effective velocity
σ	Source strength
μ	Doublet strength
b	Wing half span
C	Wing chord
C_R	Root chord
C_t	Tip chord
m	Particle mass
α	Angle of attack
R	Propeller radius
B	Propeller blade number
$r_{nacelle}$	Propeller nacelle radius
N	Number of simulated trajectories
THK	Flat plate thickness
ρ	Density

F	Prandtl factor
g	Gravitational force
K_d	Slipstream development factor
Q_∞	Freestream velocity
v'_{ia_m}	Axial induced velocity over the wing
v'_{it_m}	Tangential induced velocity over the wing
u_s, v_s, w_s	Velocity components of the particle due to source
u_d, v_d, w_d	Velocity components of the particle due to doublet
U_p, V_p, W_p	Velocity components of the particle in the global frame of reference
U_t, V_t, W_t	Freestream velocity components
Q_{AD}	Induced velocity field by the propeller
F_np	Resultant aerodynamic force
ζ	Skid angle
M_d	Dynamic moment
T	Thrust force
L	Length of the flat plate
l	Width of the flat plate
a, a'	Induction factors
n	Revolutions per minute
$X - Plan$	Coordinate of the footprint on the x axis behind the wing

INTRODUCTION

Aircraft icing is one of the main aviation's hazards that is still misconceived by many engineers due to the complex physical flow around the aircraft (Cavainolo, 2020). Icing can occur on aircraft in two manners. Firstly, ice and snow can accrete on the aircraft components when the aircraft is on the ground during cold weather. Therefore, the additional load from ice can impact on the aircraft take-off, leading to an air disaster such as in 2012 Utair flight 120 (Park, 2015). Secondly, if the aircraft is subjected to temperature lower or higher than the freezing point during flight, supercooled water droplets can freeze instantaneously, creating ice layers on the aircraft structure. The unprotected component of the aircraft subjected to supercooled water droplets within the clouds has an impact on the aerodynamic forces such as lift degradation and drag increase. Ice usually accumulates on the aircraft components such as leading edge surface at the stagnation points (Filburn, 2020). The stagnation points are the surfaces where the flow is divided between upper and lower surfaces such as the wing leading edge, the propeller, the spinner leading edge, rudder and others. (Figure 0.1) illustrates a type of inflight icing accretion on propeller blades. The ice accretion shown in (Figure 0.1) is accumulated on the propeller blade tip. Uneven additional layer of ice on the propeller blade tip can be created due to runback of the melted ice. This runback is due to centrifugal force produced by the propeller during flight operation.

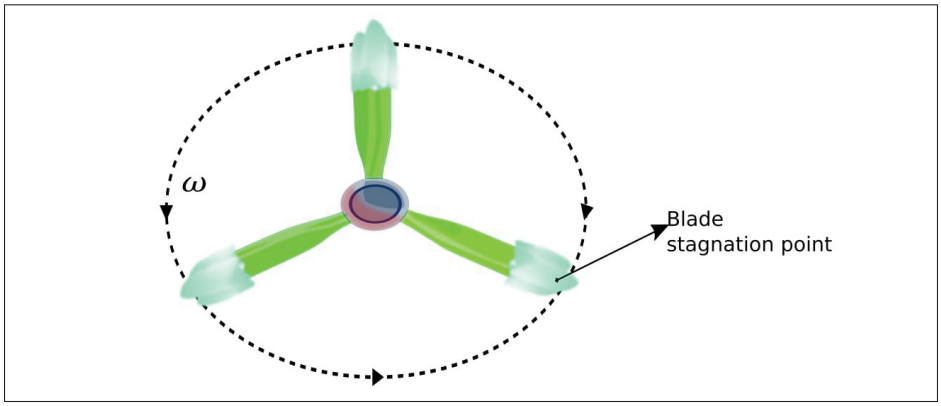

Figure 0.1 Ice Accretion on Propeller Blade Stagnation Point

The consequences of ice on the aircraft and its propeller negatively impact aircraft flight performance, causing aircraft aerodynamic instability and power losses (Liu, Li, Ning, Tian, & Hu, 2018). The Federal Aviation Administration (FAA)'s and Federal Airworthiness Regulations (FAR) Part 25 urged all the manufactures to show the ability of their aircraft to fly under icing conditions. Taking just that one measure may reduce the number of fatalities and aircraft crashes (Bond, 2009). In order to fulfill FAA requirements, the aircraft manufacturers needed to implement new systems on the aircraft body to remove the accumulated ice during aircraft flight. Various anti-icing and de-icing systems were developed to remove the excessive ice accrued weight on the aircraft components. The de-icing system removes via thermal or mechanical means any type of ice formed on the aircraft elements. One of the mechanical de-icing systems used is the pneumatic inflating boots to shed the ice accreted. They are located on the wing and on the propeller blade (Thomas, Cassoni, & MacArthur, 1996). The anti-icing systems prevent the formation of ice on the aircraft components. They use heating elements to evaporate the water droplets and avoid its frost after runback on the nearby surface. One of the examples of these heating elements is the one used by turboprop aircraft manufacturers ; the slip ring heating assembly on the propeller hub (Filburn, 2020). This heating assembly excludes all the ice accreted on the propeller root section while the propeller is operating in flight. In addition, the centrifugal force helps to remove all the additional accreted layer on the outer region of the propeller blade.

The understanding of the ice shed is still a complex task due to random accretion on the aircraft structure. During the past century, especially before 1928, the engineers faced hard challenges due to the absence of the refrigeration capabilities to create supercooled droplets to replicate inflight icing. This was caused by the cold Freon gas which was not available at this time (Filburn, 2020). Finally, after 1928, the inflight-icing hazard became more understandable by engineers thanks to, in part, advanced wind tunnel experiments. Nevertheless, the study of the ice shed for a complex wing with a propeller still remains a complicated task due to the

diverse slipstream from the wing and the propeller blade. Studying the flowfield of the wing and propeller blade is a good starting point to estimate the trajectory of the detached ice particles. (Aref, Ghoreyshi, Jirasek, Satchell, & Bergeron, 2018) validated the flowfield perturbations using the Computation Fluid Dynamics (CFD), and Reynold Averaged Navier Stokes (RANS) approach in (Figure 0.2). (Figure 0.2) illustrates the flowfield perturbation around a propeller and wing with the pressure coefficient distribution. Despite the major benefits of the propeller in accelerating a volume of air at low speed for the wings, it still has drawbacks. As can be seen from the (Figure 0.2) the slipstream interaction produced by the propeller and the aircraft flowfield itself is complex. The slipstream is the turbulent flow driven by the propeller. This complex interaction is due to additional forces and velocities added from the propeller to the slipstream behind the wing, as a result of an interference of the propeller slipstream and the aircraft slipstream.

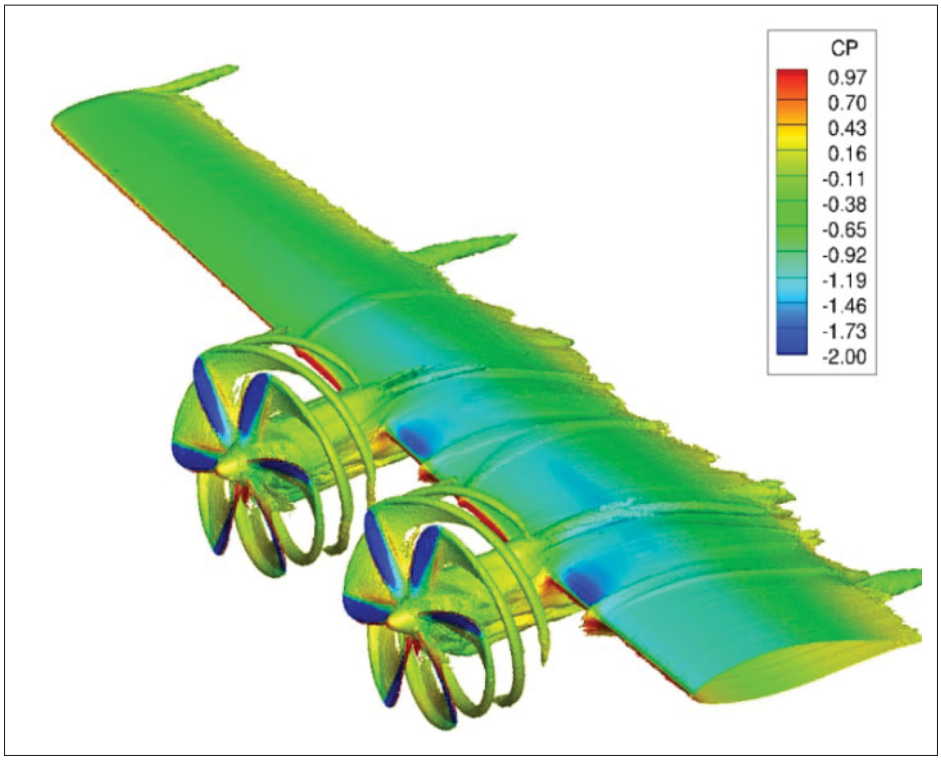

Figure 0.2 Flowfield Perturbation Around Complex Wing
Taken from Aref et Ghoreyshi (2018, p. 14)

The flying hazards obtained from the dismantled ice particles on the propeller and wing have many consequences. The detached ice particles may hit other aircraft components, reducing their safety life until failure during flight. The safety life of the components represents the ability of the components to be subjected to various load cycle without failure. In jet engines in order to prevent this issue, a probabilistic study of the flying ice particles should be taken into account to reduce the danger of ice being absorbed by the engine (Suares, 2005). This is slightly different for propellers, as the ice can hit the tail, and will need to be explored. In order to conduct the probabilistic study of the unknown ice trajectories, a configuration model of the propeller slipstream and aircraft wing interaction should be considered. Since the ice accretion is a random hazard which can appear during aircraft flights, a quantitative analysis study has to be made to create the ice shedding. A computational approach is required as well to consider all the probabilities of ice particles passage. To be able to create the ice accretion randomness for trajectory calculation, there must be a variation on the two input parameters of the ice particle. This is the initial velocity U_p, V_p, W_p , and the angle of rotation (rolling, pitching, yawing) of the ice particle.

This master thesis is aimed at studying ice shed trajectories, and quantify the effect (or non-effect) of the propeller slipstream behind the wing. This consideration is achieved by the development of a numerical tool that would merge both propeller and wing slipstream. The implementation of the numerical tool consists of a QProp model used by (Dimchev, 2012) combined with the 3D panel method used by (El Sahely, 2019). This research will serve as a step toward modelling the propeller slipstream mounted on an aircraft wing for further wing designs and propeller configurations.

Thesis objective and organization:

In order to better organize this master thesis, the following procedure will be followed. In the beginning, the main objective of this research will be described. In order to clarify and give a solution to the prediction of the unknown ice shed trajectories, a methodology will be followed. The primary objective of this thesis is to study through numerical methods the ice shed trajectories around an aircraft wing mounted with a propeller. The specific objectives are summed up and subdivided below:

- Propose a model that can study the propeller induced velocities on the wing for the ice trajectory simulation.
- Determine the pressure coefficient on the root section of the wing behind the propeller slipstream.
- Perform a parametric study on a single ice trajectory in order to observe the slipstream effect on the detached ice particle.
- Compare the obtained PDF with one without the effect of the propeller slipstream (El Sahely,2019) to observe the slipstream effect on the 1000 ice trajectories
- Compare the obtained PDF for a lower flow field velocity such that the slipstream produced by the propeller becomes more significant.

The thesis structure is subdivided into three chapters shown in (Figure 0.3) below. (Figure 0.3) is used as an introduction for the quantification of the propeller slipstream effect on the ice shed trajectory. This structure starts from the literature review of relevant methods of computation and discretization of the flow field for trajectory calculation. Then, it ends by the determination of ice passage areas around the wing. These areas have the highest probability of passage value and should be taken under further study.

The thesis structure is subdivided into three chapters shown in (Figure 0.3) below.

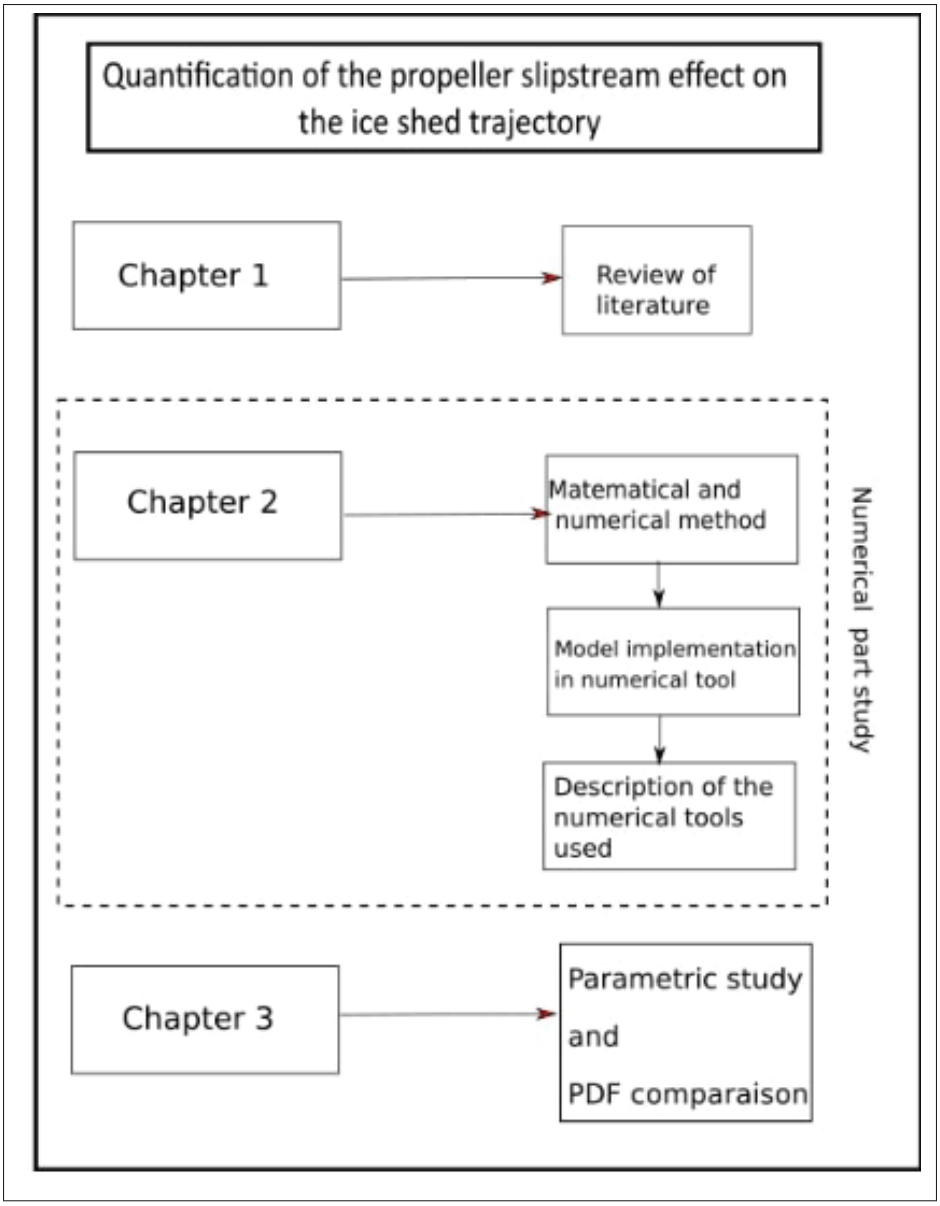

Figure 0.3 Thesis Structure

Chapter 1 presents the review of literature to provide the knowledge of icing, such as the icing effect on aircraft during flight. Also, it identifies inconstancies such as the gaps in research previously made by other researchers. It classifies the research within the context of existing literature, making a case for the importance of performing the present study. It will go over examples of computation of the ice trajectories using 3D panel method and CFD. This will help

to determine the relationship of the work in the context of its contribution to the topic. Moreover, techniques for trajectory simulation and for the PDF approach will be presented.

Chapter 2 starts with the mathematical model equations used for the trajectory computation in the flowfield. This is achieved by adding the induced velocities produced by the propeller into a 3D panel method (El Sahely, 2019). It will also explain the slipstream development model which considers the slipstream contraction over the wing. This breakthrough of the propeller slipstream is required for further flowfield correction around the wing. As well, this chapter provides the implementation of the slipstream model from Qprop (Drela, 2007) into the existing 3D panel method.The Qprop software was used and validated by (Dimchev, 2012) responsible in obtaining the axial and tangential velocities produced by the propeller. Also, a code implementation section is presented to reveal the algorithm for the interaction between the two numerical tools (Qprop-3DPM).

Chapter 3 is devoted to the parametric study test cases based on ice trajectory shed. These test cases will show the parameters which affects the dismantled ice particles. Also, the ice particle trajectory behaviour is explained with respect to the slipstream effect on it in each test case. In addition, a PDF based on 1000 trajectories is done to observe the probability of ice passage in an area. Another PDF is presented with a small flowfield velocity to see if the ice shed concentrated areas are more affected by the slipstream. Finally, a comparison of the PDF is done to quantify the effect of the propeller slipstream on the ice trajectory.

CHAPTER 1

LITERATURE REVIEW

1.1 Inflight icing hazards

The aerodynamic performance degradation of an aircraft is caused by ice accretion when flying through cloud layers, where the aircraft encounters supercooled droplets (Waldman & Hu, 2016). In addition, ice accumulation on the aircraft structure jeopardizes the aircraft safety during flight (Rausa & Guardone, 2021). The water droplets impacting upon the aircraft structure during in-flights at altitudes near freezing temperature will freeze instantaneously to form rime ice. Also, the supercooled droplets could run back as water along the wing to form glaze ice (Janjua, Turnbull, Hibberd, & Choi, 2018). The amount of accreted ice can vary depending on the component surface roughness, droplet size, aircraft speed, surrounding temperatures and other factors (Tran, Brahimi, Paraschivoiu, Pueyo, & Tezok, 1995). The studies made by (Aventin, Morency, & Nadeau, 2015) show that aircraft powered by turbo prop engines are more susceptible to icing phenomena. This assumption is deduced from a statistical study of the aircraft accident for Quebec and British Columbia between 2009 and 2014.

Inflight icing is one of the common categories of ice accretions at the source of various aircraft accidents. In order to mitigate the ice accretion hazard, different ice protection technologies are used to remove the additional layer accreted on the aircraft components. Several anti-icing technologies exist such as redirecting hot bleed air from the engine and electrothermal ice protection systems which are prop-heat, thermal heat and others (Trontin, Blanchard, Kontogiannis, & Villedieu, 2017). For a typical propeller aircraft such as the ATR72, pneumatic de-icing boots are used to shed the accreted ice (Filburn, 2020). (Green, 2006) study shows that there is a relationship between inflight incidents and ice protection systems. The inflight icing incidents, such as loss of control or stall, may result from the accretion of ice and the increase of the stall speed. The stall speed is the lowest flight speed at which the aircraft remains flyable (Cebeci, 1995).The ice shed phenomena is the detachment of the ice particle from the main aircraft body by the aerodynamic loads, the de-icing systems or both.

Due to the alteration of the aircraft speed and altitude during flight, the aircraft is subjected to various types of ice accretion which can lead to large degradation of aerodynamic performances (Andrea Rausa, Morelli, & Guardone, 2021). In order to alleviate the aircraft problems linked to ice accretion, the icing mechanism has to be presented to recognize the different types of ice accretions. (Cao, Ma, Zhang, & Sheridan, 2012) present a numerical simulation of the ice accretion on the aircraft wing. The types of ice accretion can be rime ice, glaze ice, or mixed ice, depending on the surrounding environment temperature and liquid water content. Rime ice usually accumulates at a low speed and low liquid water content. Therefore, the water droplet impinging on the aircraft structure will freeze instantaneously. Glaze ice commonly occurs at environmental temperature around $0°C$ and high liquid water content and freeze partially and flow back across the aircraft surface. (Figure 1.1) shows an example of the glaze ice accreted on an aircraft propeller, where the runback of the impinged water on the propeller blade is shown with respect to the airflow and the rotation of the propeller. In addition, the combination of the glaze ice and rime ice will give a new type called mixed ice.

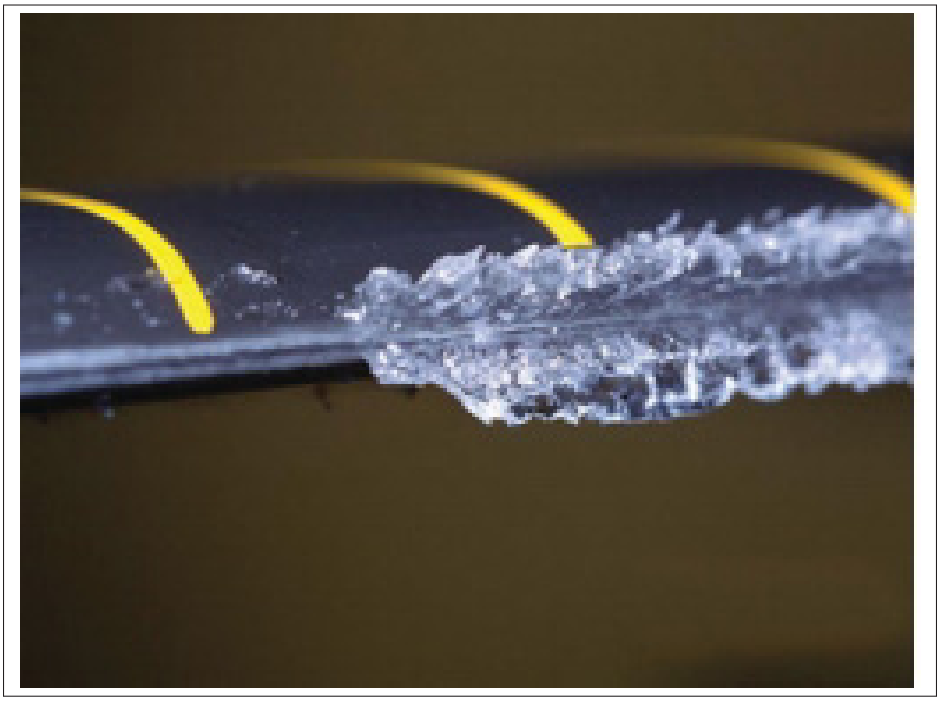

Figure 1.1 Glaze Ice Accretion on an Aircraft Turbo Prop Engine
Taken from Láoh (2015, p. 5)

1.2 Trajectory simulation of the shed ice particles.

The ice shedding study is critical due to the significant degradation of aircraft aerodynamic performance and engine clog during aircraft operation (Trontin, Blanchard, Kontogiannis, & Villedieu, 2017). This section presents the previous simulations and studies of the ice shedding made by some researchers from the literature. These studies are based on various methods. This section will mention only the most common and the ones which predict the ice shedding result with fewer errors.

Considering the tremendous expenses required to perform flight test cases to study the ice shedding phenomena, two analogous forms of trajectory simulation methods have been presented by researchers. The first method performs wind tunnel test cases. This method is still being a bit far from the realistic results due to the impossibility to recreate all dimensionless parameters such as the one in the actual flight (Horák, Rozehnal, Chára, & Hyll, 2008). Beside that, wind tunnel tests have been carried out by the researchers and manufacturers since the beginning of aerospace industry due to the controllable environment they can establish. Researchers have made some experiments in order to get a clearer picture of the ice accretion physics and shapes. (Addy Jr et al., 2016) have provided databases from wind tunnel from the study SUNSET (StUdies oN Scaling EffecTs due to ice) project. The ice accretion simulation studies are done on a two-dimensional (2D) NACA23012 airfoil. In addition (Papadakis, Yeong, Wong, Vargas, & Potapczuk, 2005), and NASA such as (Currie, Fuleki, Knezevici, & MacLeod, 2013) provided some databases. These databases were intended to obtain a model to feed their numerical code for the ice shedding. Moreover, Jacob, J. (2006) obtained force and moment coefficients for ice fragments (rectangular flat plate, a semi-circular shell, and a hemispherical shell) using 6-DOF wind tunnel tests. Depending to yaw, pitch, and roll orientations, the experimental results revealed considerable changes in the aerodynamic properties of the ice particles studied.

(Shimoi, 2010) used both experimental and computational methods to study ice shedding and ice trajectory. the 6-DOF model used replicates the trajectory of a square plate, a rectangular flat plate, and a disk-shaped ice pieces.

Another method for trajectory simulation is the computational method or the so-called cost-

effective method (Horák, Rozehnal, Chára, & Hyll, 2008). In order to understand the complex flowfield on the aircraft near ice accumulation, various methods for flowfield computations are proposed. These methods helped manufacturers to improve their ice protection systems. Also, those analyses showed the importance of implementing additional heating pads on the aircraft structure (Láoh, 2015). Heating pads keep the impinged ice structure as clean as possible during flight. In addition, the trajectory method simulation helped predict the unknown trajectories resulting from the detached ice particles and damaging the surrounding aircraft components.

The Panel Method (PM) is a common method used to predict the flowfield around any arbitrary body. The PM gives good numerical results in a short computation time. For potential flow problems PM is used (Katz, Joseph, Plotkin, & Allen, 2001). The calculation of the flowfield parameters will allow to compute the trajectory. (Özgen & Canıbek, 2012) used a two-dimensional Hess-Smith PM to compute the flowfield. (El Sahely, 2019) used a numerical approach based on three-dimensional PM to calculate the random trajectory around a NACA0012 airfoil. Also, another common method is the vortex lattice method (VLM) used by (Dimchev, 2012).

Similar methods used also a CFD flow field. Santos, Papa, et Do Areal Ferrari (2003) used a CFD solution from FLUENT to model ice trajectories. The trajectories are determined utilizing literature-based correlations for aerodynamic coefficients. The ice was shed from a fixed point with coordinates of x = -0.1 m, y = 0.1 m, and z = 0.1 m. Furthermore, Baruzzi et al. (2007) used CFD to develop a new approach for modelling ice shed trajectories inside a homogeneous flow field. The research used a Navier-Stokes analysis with implicit linearization and finite element discretization. The simulation is built on shifting sub-meshes within the main mesh that are stitched together. Moreover, using a CFD flowfield, Ignatowicz et al. (2019) investigated the ice trajectories around a blended wing body aircraft. For the sphere and the flat plate ice shapes, a Lagrangian technique was used to simulate ice block movement. As well, (Papadakis, Yeong, Suares, 2007) simulated ice shedding by coupling numerical computerized simulations with experimental wind-tunnel data. The aerodynamic coefficients of ice fragments are determined using experimental data, after which they are imported into the numerical model.

1.3 Propeller slipstream and fixed-wing interference

Until now, numerical studies of the ice shedding were conducted without considering the propeller effect. Neither of the studies (Papadakis, Yeong, Suares, 2007), Baruzzi et al. (2007) considered the major drawback of the propeller icing on the aircraft which can lead to aircraft imbalance or inability to maintain flight due to lack of power from engines. The inefficient performance from the engine is due to accreted ice loads on the propeller blade. Ice slabs affected by the slipstream behind the propeller could hit the aircraft components (Mingione, Barocco, Denti, Bindi, & French, 1997), causing a major issue. The slipstream is the airflow driven in the backward direction by the propeller, can shed the ice at high velocity due to centrifugal forces produced by the propeller. The influence of the propeller on the turbo-prop aircraft is always significant in the aerodynamic performance. The propeller wake induced velocities in all directions on the other aligned aircraft components. The aircraft wing is at the same time considered to possess a blockage effect on the propeller slipstream and change the inflow magnitude. Also, this blockage effect by the aircraft wing can change the propeller distribution of thrust and torque (Ying, Liang, Shuo, & Xinglin, 2015). (Witkowski, Lee, & Sullivan, 1989) described the influence of the propeller slipstream on a wing. As the propeller rotates, a swirl is obtained which directly affect the wing in the propeller slipstream. In this case, the result will be the creation of upwash and downwash regions (increase of the lift coefficient) resulting in a thrust force (negative drag force). In the literature, a large amount of researcher tried to take into account the aerodynamic effect of the interference of the propeller and wing and the challenge is to achieve an accurate numerical study of the propeller slipstream.

(Glauert, 1935) showed the rotor exposition of varying azimuthal inflows close to the wing, leading to a severe increase in the angle of attack of the propeller blade. (Droandi & Gibertini, 2012) used a method by Conway (ring vortex) to give a general solution for actuator disk. The propeller and its wake are modelled by means of a system of vortices. The superposition of an appropriate vortice distribution gives the actuator disk model. The actuator disk solution is given by axial and tangential induced velocities considering a PM is used to calculate the flowfield. A good agreement was obtained by the actuator disk. However, the real configuration

of the blade is not described and it can lead to grid generation difficulties.

The rotor model was simply inserted to create disturbance in the wing onset flow. However (Lotstedt, 1992) took fully into account coupling and created a propeller slipstream model. This slipstream model is added to a wing PM. The result of that early age was not accurate due to the lack of performance of the computing machine on prop/wing coupling code due to complexity and massive number of elements. The model for (Lotstedt, 1992) carried out strong singularities in the external flow to achieve better results.

In the case of a complex wing with vorticial problems behind the rotating propeller, PM can be amended as well (Lotstedt, 1992). (Dimchev, 2012) used a combination of vortex lattice method (VLM) from (Katz et al., 2001) with the Blade Element Momentum Theory (BEMT). The propeller implementation in the VLM was done by introducing a velocity component at the control point with the free stream velocity. (Li, Lu, & Deng, 2014) used an actuator disk model to couple momentum and the Blade Element Momentum Theory (BEMT). BEMT is used to compute force at any section of the blade. The pressure jump in the disk is the propeller produced thrust per unit of the disk. Their method focused more on defining axial and tangential velocities. From velocities, the thrust and torque of the actuator are obtained for implementation in pressure jump and tangential induced velocity.

The consequences of ice on the aircraft propeller has a crucial impact on the flight condition (Favier, Ettaouil, & Maresca, 1989). The recent experimental study made by (Liu, Li, Ning, & Hu, 2017) on the propeller ice accretion shows a decrease in aerodynamic performance and stability of the aircraft. Modelling the propeller is a complex task, due to the rotation of the propeller blade which causes a highly unsteady flow field.

The objective of this thesis is to build a tool that is capable of making a fast study of the propeller and wing geometry on the footprint map. The theoretical approach to the rotor/airfoil problem uses the PM of (Katz et al., 2001) for the wing developed by (El Sahely Hassan, 2019). The method used to obtain the flow field around the wing is a 3D-based PM (3DPM). Additionally, the Qprop advanced BEMT program made by (Drela,2007) is employed to determine the induced velocities to represent the slipstream. A mathematical model and numerical method is required for the coupling between the propeller and the wing.

CHAPTER 2

MATHEMATICAL MODELING AND NUMERICAL METHOD

This part of the thesis describes the approach proposed for the ice shedding trajectory computation behind a wing with a turbo-prop engine. This part is split into 3 subsections:

- The first subsection describes the mathematical model which compute the flowfield using the 3D panel method (3DPM).
- The second subsection outlines the numerical method adopted for the approach used to implement the propeller induced slipstream in the flowfield. Moreover, it presents the ice trajectory computation behind the aircraft slipstream.
- The third section defines the numerical tools used for the ice trajectory simulations, as well as the code implementation in (QProp) and MATLAB. At last the PDF is pointed out for the ice footprint map.

2.1 The Mathematical Model

The first step is to define the mathematical model for the flow field calculation using the 3D panel method (3DPM). An efficient model of propeller effect is embedded in the PM code. The 3DPM allows computing all the velocities at all point on the solid body as well as in the far field (Walchner, 1937) . For this typical prop/wing analysis, a PM was chosen over the vortex lattice method (VLM). Moreover, it gives low computational time with acceptable results of forces and velocities (Gamme, De Oliveira Andrade, Ragni, & Lau, 2017). Also, PM takes into account the wing thickness compared to VLM.

2.1.1 3D Panel Method

The model for the flow field calculations using the 3DPM is explained. The model follows the method of (Katz & Plotkin, 2001) for potential flow around a solid body. The shed ice trajectory is treated in an irrotational, inviscid and incompressible flow.

Firstly, equation (2.1) describes the potential flow around a solid body.

$$\Phi = \phi + \Phi_\infty \tag{2.1}$$

where, ϕ is the perturbation potential velocity and Φ_∞ is the fluid potential is given by the equation (2.2).

$$\Phi_\infty = U_\infty.x + V_\infty.y + W_\infty.z \tag{2.2}$$

where, $(U_\infty, V_\infty, W_\infty)$ are the freestream velocity components.
The velocity of the flow field can be obtained from the derivative of a potential which fulfills Laplace's equation (2.3):

$$\nabla^2\Phi = 0 \tag{2.3}$$

This Laplace equation (2.3) can be solved as long as the boundary condition satisfies equation (2.4).

$$\nabla\Phi.n = -V_\infty.n \tag{2.4}$$

The boundary conditions equation (2.4) was originally taken from (Katz & Plotkin, 2001). It was under the form of equation (2.5) which consider any velocity in the normal direction on the airfoil is zero

$$\nabla\Phi.n = 0 \tag{2.5}$$

2.1.2 Blade Element Theory (BEMT)

The Blade Element Momentum Theory (BEMT) is a mathematical model to determine the behaviour of the propeller. It can estimate the forces acting on a propeller blade. The BEMT assumes that the forces acting on the airfoil can be constructed from the aerodynamic forces acting on a blade. It is also assumed that there is no interference in the propeller sequential blades. Moreover, the induced velocity components (v_t, v_a) are used to describe the tangential and axial velocity induced by the propeller.

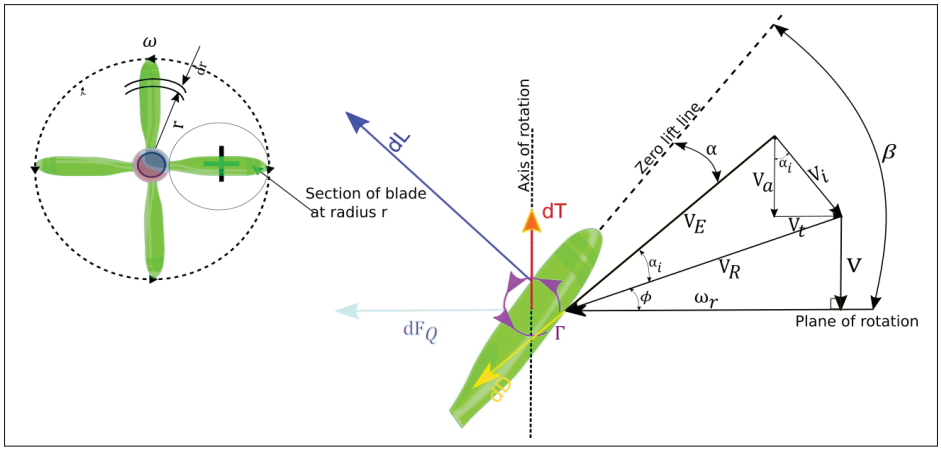

Figure 2.1 Velocity and Eorces Acting on a Four Blade Propeller
Inspired by McCormick (1995)

(Figure 2.1) illustrates the velocity and forces acting on the blade propeller rotating in anticlockwise direction, inspired from (McCormick, 1995).The effective velocity v_E with axial v_a and tangential v_t is the velocity clearly acting on the propeller. The theory is based on the momentum conservation law enforced between $(r, r + dr)$ circular stream tubes. The conservation law is applied in two directions, giving respectively axial and tangential equations (2.6-2.7). For axial direction

$$2\pi dr\rho(V + \bar{v_a})\bar{v_{a3}} = dT_0' \tag{2.6}$$

For tangential direction

$$2\pi dr\rho(V+\bar{v_a})\bar{v_{t3}} = \frac{dQ'_0}{r} \tag{2.7}$$

where subscript 3 refers to far downstream of the propeller and V is the free stream velocity. dT'_0 is the thrust and it is given in the following equation (2.8)

$$dT'_0 = BdL\cos(\phi+a_i) = BC_l(\frac{1}{2\rho v_e^2 cdr})\cos(\phi+a_i) \tag{2.8}$$

where dL is the force acting on the blade component multiplied by (B) the number of blade element. $\frac{dQ'_0}{r'}$ is the torque and its given by equation (2.9)

$$\frac{dQ'_0}{r'} = BdL\sin(\phi+a_i) = BC_l(\frac{1}{2\rho V_e^2 cdr})\sin(\phi+a_i) \tag{2.9}$$

Therefore, the effective velocity vector can be written as equation (2.10):

$$v_e = \frac{V(1+a)}{\sin(\phi+a_i)} = \frac{\Omega r(1-a')}{\cos(\phi+a_i)} \tag{2.10}$$

where, (a, a') are the induction factors and they are given by the following equations
$a = \frac{v_a}{V}$ and $a' = \frac{v_t}{\Omega r}$

2.1.3 Prandtl tip loss factor

Adding the thin propeller geometry to the airfoil will require a tip loss correction for the propeller blade (Glauert, 1935). The Prandtl factor is required for better approximation result near the tip (Ramdin, 2017). This factor F is given by the approximation of the axial and tangential velocities equation (2.11).

$$\frac{\bar{v_a}}{v_a} = \frac{\bar{v_t}}{v_t} = \frac{\bar{v_{a_3}}}{v_{a_3}} = \frac{\bar{v_{t_3}}}{v_{t_3}} = F \tag{2.11}$$

where,

$$F = \frac{2}{\pi} \cos^{-1}\left(e^{-f}\right) \tag{2.12}$$

The final form after rearrangement of equations (2.8-2.11) into equation (2.6-2.7) will give the equations for the axial and tangential directions.

2.1.4 BEMT and PM coupling

The method is described by (Giovanni Droandi & Gibertini, 2012) which included the propeller within a 3DPM. The coupling between PM and BEMT modification begin with equation (2.4). The main modification occurs on the right-hand side of the equation by introducing the velocity induced by an actuator disc. Therefore, the PM equation becomes equation (2.13).

$$\nabla\phi.n = -(Q_\infty + Q_{AD}).n \tag{2.13}$$

where, Q_∞ is the freestream velocity field.
As mentioned above, the fact of adding the propeller disc to the PM will add a velocity field induced by the propeller Q_{AD} on the right-hand side of the Cartesian coordinates.

2.1.5 Propeller slipstream over the wing

In a holistic perspective, it should be taken into account that the slipstream varies from the propeller plane to the wing. (Hunsaker, 2007) studied this effect and revealed the change of the slipstream by contraction. This contraction creates the increase of the tangential and the axial induced velocities. In addition, another study performed by (Stone, 2008) employed a similar

slip stream development model. This fulfillment was made into the MATLAB trajectory code from (El Sahely, 2019) by implementing the slipstream development factor. The new MATLAB function created will be calle trajectory panel method (TRAJPM).
The slipstream development factor K_d equation (2.14) appropriated from (McCormick, 1999).

$$K_d = 1 + \frac{s}{\sqrt{s^2 + R^2}} \tag{2.14}$$

where, (s) is defined as the distance between wing mid-chord and propeller plane. In addition, some equations should be added to the TRAJPM to describe and scale the velocities. (Stone, 2008) clarified the possibility of obtaining the slipstream by applying the mass and momentum conservation equations. At the end, the slipstream tube and the distribution of the velocities are defined in equation (2.15).

$$r_m^{prime} = \left\{ \frac{r_{nacelle}}{\sqrt{r_{m+1}^2 + (r_m'^2 - r_{m-1}^2)K_v}}, m = 1...n \right. \tag{2.15}$$

where, m is the number of propeller inner radius division and K_v is given below.

$$K_v = \frac{\left[2V_x + v_{ia_m} + v_{ia_{m-1}}\right]}{\left[2V_x + K_d(v_{ia_m} + v_{ia_{m-1}})\right]} \tag{2.16}$$

Figure 2.2, inspired by (Stone, 2008) shows all the radius distribution from the slipstream expansion, to better reflect the slipstream tube equations (2.14-2.15).

The following equations (2.17-2.18) show the resulting induced velocity components over the wing v'_{ia_m} for axial and v'_{ia_t} for tangential.

$$v'_{ia_m} = K_d v_{ia_m} \tag{2.17}$$

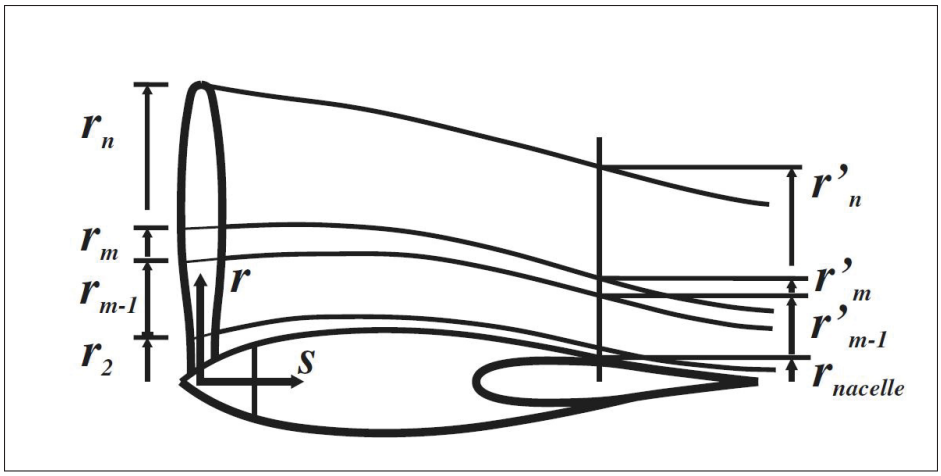

Figure 2.2 Slipstream Development Quantities
Taken from Stone (2008, p 201)

$$v'_{ia_t} = 2v_{it_m}(\frac{r_m}{r'_m}) \tag{2.18}$$

where, the induced velocity components v_{ia_m} and v_{it_m} are obtained using the BEMT. Also, r_m and r'_m are the propeller inner radius at the propeller area and after the slipstream development above the wing.

(Stone, 2008) showed that the development of the axial velocity is proportional to the slipstream development factor k_d. Consequently, the value of the tangential velocity is double after the propeller; this is due to the conservation of the angular momentum.

Figure 2.3 gives the illustration of how both axial and tangential induced velocities are added to the freestream velocity component. This step is required to provide the flowfield over the wing panels in the boundary condition equation (2.4).

It should be clarified as well that the assumption made by (Stone, 2008) for coincidence of slipstream with propeller axis should be considered. Otherwise, the slipstream will be blown away from the wing.

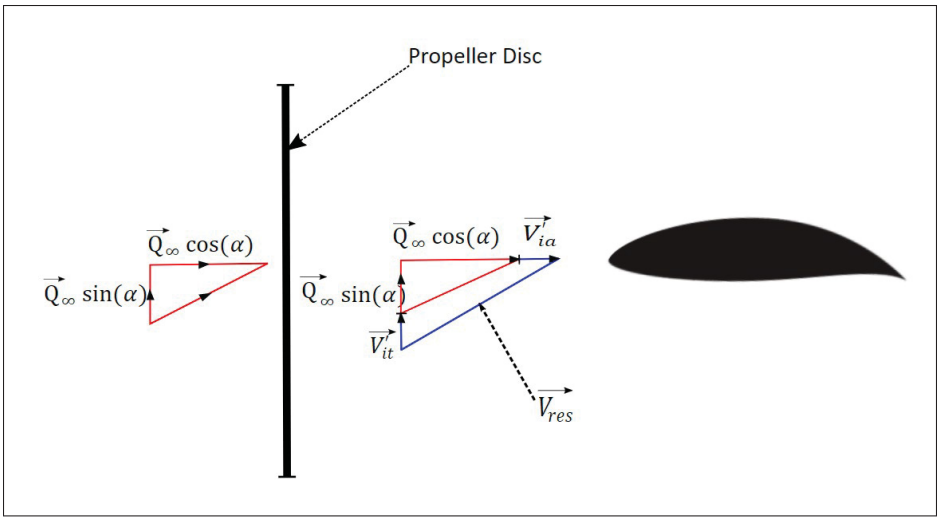

Figure 2.3 Velocity Diagram : Upgoing Blade Side of the Propeller Inspired by Stone (2008)

2.1.6 Dirichlet's boundary condition

The integral equation uses a combination of constant sources panels and doublets to represent the wake. The source panels with strength (σ) and the doublet strength source μ is fixed and constant. Therefore, the integral equationwill give a set of equations with the unknown doublet strength equation (2.19).

$$\sum_{j=1}^{N_s} B_j \sigma_j + \sum_{j=1}^{N_v} C_j \mu_j = Q_\infty . n \tag{2.19}$$

where, N_s and N_v are the numbers of sources and doublets panels. B_j and C_j represent the influence coefficient matrices acting as the influence of sources and doublets distribution. n is the normal direction on the surface. The equation (2.19) is a discretized linear equation without coupling of the propeller yet.

The source strength equation (2.20) is given by (Katz & Plotkin, 2001).

$$\sigma_j = Q_\infty . n \tag{2.20}$$

where Q_∞ is the freestream velocity.

After introducing the propeller solution into equation (2.19), the final expression of the discretized linear equation is given by the equation (2.21).

$$\sum_{j=1}^{N_s} B_{1j}\sigma_j + \sum_{j=1}^{N_v} C_{1j}\mu_j = (Q_\infty + Q_{AD}).n \tag{2.21}$$

It is important to mention that this model only takes into account the effect of the propeller slipstream on the wing and not vice versa. Though (Veldhuis, 2005) implemented the aerodynamic effect of the wing on the propeller but it will not be employed in this study. The reason is that the correction is assumed to have no effect on the PDF studied behind the wing.

2.1.7 Influence coefficient matrix

The equation (2.21) mixed with the boundary condition, transform into the matrix form equation (2.22). The following equation (2.22) shows a set of m linear equation. The source elements on each panel are known from equation (2.20) (Katz & Plotkin, 2001).

$$\begin{bmatrix} a_{11} & a_{12} & \dots & a_{1m} \\ a_{21} & a_{22} & \dots & a_{2m} \\ a_{31} & a_{32} & \dots & a_{3m} \\ \vdots & \vdots & \ddots & \vdots \\ a_{m1} & a_{m2} & \dots & a_{mm} \end{bmatrix} \begin{bmatrix} \mu_{11} \\ \mu_{21} \\ \mu_{31} \\ \vdots \\ \mu_{m1} \end{bmatrix} = - \begin{bmatrix} \sigma_{11} \\ \sigma_{21} \\ \sigma_{31} \\ \vdots \\ \sigma_{m1} \end{bmatrix} \begin{bmatrix} b_{11} & b_{12} & \dots & b_{1m} \\ b_{21} & b_{22} & \dots & b_{2m} \\ b_{31} & b_{32} & \dots & b_{3m} \\ \vdots & \vdots & \ddots & \vdots \\ b_{m1} & b_{m2} & \dots & b_{mm} \end{bmatrix} \tag{2.22}$$

where, a_{jj} is the influence coefficient and the right-hand side (RHS) component are given by equation (2.23)

$$\begin{bmatrix} a_{11} & a_{12} & \dots & a_{1m} \\ a_{21} & a_{22} & \dots & a_{2m} \\ a_{31} & a_{32} & \dots & a_{3m} \\ \vdots & \vdots & \ddots & \vdots \\ a_{m1} & a_{m2} & \dots & a_{mm} \end{bmatrix} \begin{bmatrix} \mu_{11} \\ \mu_{21} \\ \mu_{31} \\ \vdots \\ \mu_{m1} \end{bmatrix} = \begin{bmatrix} RHS_1 \\ RHS_2 \\ RHS_3 \\ \vdots \\ RHS_m \end{bmatrix} \tag{2.23}$$

2.1.8 Velocity computation

One of the main benefits of the PM is the ability to compute surface velocities at each panel. The assessment of these velocity magnitudes is based on known doublet and sources elements from (Katz & Plotkin, 2001). In order to determine the velocity around an aircraft wing on a point of interest $P(x, y, z)$ in the far field, each panel on the wing should be considered. The aircraft wing in this study possess more than one panel either chordwise or spanwise. Therefore, the summation of the influenced velocities on each panel at the point of interest P will be done and the velocity component will be determined on two elements.

The first velocity will be calculated based on the source element equation((2.20) from (Katz & Plotkin, 2001).

$$u_s(x, y, z) = \frac{\sigma A(x - x_0)}{4\pi[(x - x_0)^2 + (y - y_0)^2 + z^2]^{\frac{3}{2}}}$$

$$v_s(x, y, z) = \frac{\sigma A(y - y_0)}{4\pi[(x - x_0)^2 + (y - y_0)^2 + z^2]^{\frac{3}{2}}} \tag{2.24}$$

$$w_s(x, y, z) = \frac{\sigma A(z - z_0)}{4\pi[(x - x_0)^2 + (y - y_0)^2 + z^2]^{\frac{3}{2}}}$$

where, A is the panel area and (x_0, y_0, z_0) are the coordinates of the collocation point coordinates of the panel z_0. (u_s, v_s, w_s) are the velocity potential due to the source element.

The second velocity will be calculated based on the doublet element equation from (Katz & Plotkin, 2001).

$$u_d(x,y,z) = \frac{3\mu A(x-x_0)z}{4\pi[(x-x_0)^2+(y-y_0)^2+z^2]^{\frac{5}{2}}}$$

$$v_d(x,y,z) = \frac{3\mu A(y-y_0)z}{4\pi[(x-x_0)^2+(y-y_0)^2+z^2]^{\frac{5}{2}}} \tag{2.25}$$

$$w_d(x,y,z) = \frac{\mu A[(x-x_0)+(y-y_0)^{-}2z^2]}{4\pi[(x-x_0)^2+(y-y_0)^2+z^2]^{\frac{5}{2}}}$$

where (u_d, v_d, w_d) are the potential velocities coordinates due to the doublet element, μ is the doublet strength and A is the panel area.

To obtain the total fluid velocity surrounding the wing behind the propeller section, the induced velocities are added to the wing panel elements (source-doublet) in x-direction. The summation of the axial induced velocity component in the x-direction signifies the induced velocity effect by the propeller. Therefore, the total fluid velocity behind the propeller in the x-direction is shown in equation (2.26).

$$U_{total}(x,y,z) = U_\infty - u_s(x,y,z) - u_d(x,y,z) + v'_{ia_m} \tag{2.26}$$

where, $U_{total}(x,y,z)$ is the fluid velocity in x-direction, U_∞ is freestream velocity component in x-direction, $u_s(x,y,z)$ is the velocity component due to source, $u_d(x,y,z)$ the velocity component due to doublet and v'_{ia_m} the axial induced velocity over the wing.

Also, to represent the influence of the propeller in the y-direction the summation of the tangential induced velocity component to the wing elements (source-doublet) in y-direction is done. Therefore, the total fluid velocity surrounding the wing behind the propeller the y-direction is represented by the following operations in equation (2.27).

$$V_{total}(x, y, z) = V_{\infty} - v_s(x, y, z) - v_d(x, y, z) - v'_{ia_t} \tag{2.27}$$

where, $V_{total}(x, y, z)$ is the fluid velocity in y-direction, V_{∞} is freestream velocity component in y-direction, $v_s(x, y, z)$ is the velocity component due to source, $v_d(x, y, z)$ the velocity component due to doublet and v'_{ia_t} the tangential induced velocity over the wing.
The radial induced component is directed normal to the page with a small contribution. Therefore, the radial induced velocity v'_{ia_r} component is neglected in this calculation simular to (Dimchev, 2012). The fluid velocity around the wing with the propeller in the z-direction is represented by the following operations in equation (2.28).

$$W_{total}(x, y, z) = W_{\infty} - w_s(x, y, z) - w_d(x, y, z) \tag{2.28}$$

where, $W_{total}(x, y, z)$ is the fluid velocity in y-direction, W_{∞} is freestream velocity component in y-direction, $w_s(x, y, z)$ is the velocity component due to source and $w_d(x, y, z)$ velocity component due to doublet.

2.1.9 Monte Carlo simulation and PDF estimator

Since aircraft ice shedding is a complex task that requires the setup of random initial conditions for the ice trajectory shed (El Sahely, 2019) suggested the Monte Carlo simulation. Monte Carlo simulation allows for the initial uncertainties created by the ice shedding. This method was previously used by (Papadakis, Yeong & Suares, 2007) and it allows obtaining a probability of ice passage behind the wing. The algorithm used in this method is based on the multiple trajectory calculation. Nevertheless (Papadakis, Yeong, & Suares, 2007) mentioned one deficiency of this method, which is the massive number of trajectories around 30,000 to obtain relevant results. Therefore, (El Sahely, 2019) assumes a PDF shape to decrease the number of the computed trajectories.
To replicate the conditions for the Monte Carlo trajectory calculation, it is needed to set variable

parameters which can be: initial shed sections, initial orientation of the ice particle, ice particle dimensions, angular velocity, linear velocity and other parameters. The two variables to be varied in this study are the ice particle initial velocity (U_p, V_p, W_p) and the initial orientation depending on the Euler angle (roll, pitch, yaw). The choice of these two parameters for this study is similar to (El Sahely, 2019) and is intended for future parametric study and PDF comparison. The detailed equations of the varied parameters for the Monte Carlo approach are available in the work of (Ignatowicz et al., 2019) and (El Sahely, 2019).

(El Sahely, 2019) proposed a method which can presume the shape of the PDF to decrease the number of trajectories required. This method allows reducing the computation time of the huge trajectory simulations for Monte Carlo simulation.

Since the ice footprint in this study are collected in Y and Z coordinates, several assumptions are made similar with the one of (El Sahely, 2019) to predict the PDF. These assumptions are made in favour of reducing the complication of the 3DPDF distribution. The first assumption is that the probability along Y-axis $P(Y)$ is assumed to have normal distribution. The second assumption is that the probability along Z-axis $P(Z)$ is assumed to have Binormal distribution. $P(Y)$ and $P(Z)$ are the projections of the 3D distribution along the Y and Z-axis. Also, the PDF estimator mathematical approach is available in the work of (El Sahely, 2019).

2.2 Numerical tools acceptance

This section will cover all the numerical tools used in this study to determine the ice trajectory around the wing behind the propeller. Two numerical tools are used in this study: Qprop and a TRAJPM. Qprop is used to evaluate all the induced velocities along the propeller inner radius. The TRAJPM is used to compute the ice trajectories in nonuniform flowfield with propeller slipstream. Further explanation will tell on the QProp propeller analysis program and the TRAJPM is used for the computation of the ice particle.

2.2.1 QProp background information

In order to obtain propeller analysis data, a numerical tool is required in this prop/wing study. (Drela, 2007) offered an open source code under public license, which can be used by anyone and is available as a free software. Also, this program showed its simplicity and reliability with different engine parameters (Lowe, 2015). This BEM moment analysis program was used as well in (Dimchev, 2012) studies. A propeller-motor combination is chosen for the study to produce the induced velocity behind the wing, and to represent the slipstream produced by the propeller during flight.

To give a general idea of QProp, the program consists of a motor model and a propeller aerodynamic model. (Drela, 2007) described Qprop theoretical aerodynamic formulation. As it was pointed up above, this program follows the classical blade element/vortex formulation from (Goldstein, 1929). The program was then modified by (Dimchev, 2012) for adjustments of motor and propeller parameters. Those adjustments have provided the induced velocities by using some inputs arranged in chapter 3 as tables of initial parameter for the ice trajectory simulation.

2.2.2 TRAJPM MATLAB toolbox

A mathematical model for ice trajectory computation has been implemented in MATLAB (El Sahely, 2019) for the aircraft wing possesing a NACA0012 airfoil. It is called TRAJPM. The TRAJPM is used for the non-uniform flowfield trajectory calculation. The benefits offered by this program are obtaining multilpe trajectories analysis as well as a visualization of the footprint map PDF. Additionally, building upon this existing program is advantageous to reduce time spent coding from scratch and dedicate more time to the models rather than their implementation. Random number generator is used in this study to create different values for the intial shed parameters (initial ice particle angle and intial particle velocity). MATLAB comes with a set of effective built-in algorithms that allow for a wide range of calculations. It also includes simple graphics commands that allow for fast viewing of results. Potential features are combined together in toolbox packages: Data processing, symbolic computation, communication theory, enhancement, and a variety of other sectors of applied fluid mechanics which do have techniques

and algorithms.

Also, MATLAB supports syntax programming and has advanced analytical structures (Higham, D, 2016). It also features built-in coding and debugging capabilities. Because of these functionalities, MATLAB seems to be an outstanding strong research tool.

2.3 Code implementation

This part of the thesis show the process of coupling (QProp) and TRAJPM, for the ability to compute the flow around an aircraft wing with a turboprop engine. This section is essential in order to study the propeller effect on the shed ice trajectory from the aircraft wing.

(Figure 2.4) shows the algorithm used for the coupling between the propeller and the ircraft wing. The aircraft wing is based on the (NACA0012) airfoil. For better description of this implementation, the (Figure 2.4) is subdivided into three parts:

- The first part which is designated under the letter (a), give the input data required for the (QProp) program to run. These input data are the engine and propeller characteristics. Thus, the program output a (Velocity.txt) file which contains all the induced velocity components on the radial section of the blade. The program main advantage is the advanced BEMT analyses which give different induced velocities depending on the inner radius of the blade. This means the induced velocities produced by the propeller will increase starting from the inner radius propeller hub to the propeller tip.
- The second part in (Figure 2.4) is designated under the letter (b). This part is relevant since (Stone, 2008) has shown that the magnitude of the slipstream induced velocities produced by the propeller doesn't remain constant when it reaches the wing area. This part consists of a MATLAB function which gives the modifications of the propeller induced velocities originally based on Stone slipstream development equations and slipstream factor (K_d). Therefore, the obtained induced velocities on the radial section of the wing will be transformed into proper induced velocities (axial-tangential) above or below the wing section.
- The third part is designated under the letter (c). It contains the implementation of the obtained induced velocities from the second part (b) in the fluid velocity equation used by

(El Sahely, 2019). Each ice particle located in the slipstream area will gain an additional induced velocity from the propeller placed in front of the wing. The main modification is performed in the (Veloc.m) TRAJPM.

After coupling the propeller model with theTRAJPM code, the same implementation is performed for a single ice trajectory parametric test case study. Moreover, the resulting footprint map coordinates (Y-Z) obtained from the ice trajectory simulation is saved in matrix form. These footprint map coordinates are used for the PDF for later visualization of the ice shed concentrated area. Also, these footprint maps are used for the PDF comparison with the one available in the literature to verify the effect of the propeller slipstream on the ice trajectory.

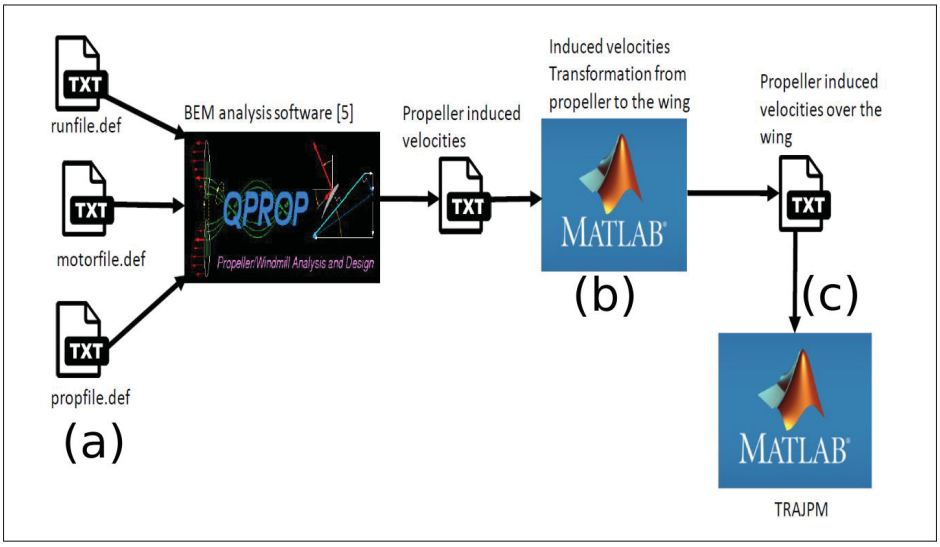

Figure 2.4 General Coupling of the Prop-Wing Methodology for the Ice Trajectory Simulation

CHAPTER 3

PARAMETRIC STUDY AND PDF STUDY

The ice accumulations on aircraft various surfaces lead to the creation of ice fragments. Different shapes of ice fragments can be created by the accretion phenomena depending on the effectiveness of the inboard ice protection systems. Another contributing factor is the delayed activation of these protective systems by the pilot during aircraft operation. Various test cases will be performed in order to determine the parameters which affect the ice particle trajectory shed from the aircraft wing with a turboprop engine.

Therefore, this following chapter will be subdivided into three sections:

- The first section compares the pressure coefficient (C_p) on the NACA0012 airfoil with the propeller slipstream and the pressure coefficient achieved by (El Sahely, 2019). The (C_p) computation will be on the root section of the wing build from a (NACA0012) airfoil.
- The second section will be a parametric study based on 6 test cases on a single ice trajectory. These test cases are intended to show the parameter effects on the trajectory since the ice chunks can be shed randomly. It will help gain a better understanding of the effect of the slipstream on the ice trajectory.
- The third section will present the Probability Distribution Function (PDF) obtained from 1000 trajectories with the propeller slipstream. The PDF of the trajectory footprint is one of the main tools to see the effect of the slipstream effect on the flying melted ice particle. The result of the PDF will reveal if the ice footprint concentrated area are higher than the one computed by (El Sahely, 2019). In addition, this section will consider another PDF where the propeller slipstream will be more significant on the aircraft velocity.

3.1 Pressure coefficient distribution

This section describes the pressure coefficient distribution (C_p) on the aircraft wing based on a NACA0012 airfoil . The wing has a chord length of $1m$ and an aspect ratio value of 10. In order to determine the pressure distribution coefficient along the wing section, the wing should be

discretized into panels (Chordwise-Spanwise). In order to compute the pressure distribution using 3DPM, an approach similar to the one of (El Sahely, 2019) is used.

This wing span for this study is equal to $10m$. (Figure 3.1) illustrate the concept of computing the pressure coefficient (C_p) distribution on the NACA0012. The propeller is shown in the figure at the shed location $Y = 3m$. Three (C_p) are collected to identify the pressure distribution changes along the wing. C_{p1} gives the pressure distribution on the spanwise panel root section of the wing. C_{p2} gives the pressure distribution behind the spanwise panel propeller slipstream . C_{p3} provide the pressure distribution on the spanwise wing tip.

The pressure distribution result obtained from (Figure 3.1) is shown in (Figure 3.2) .

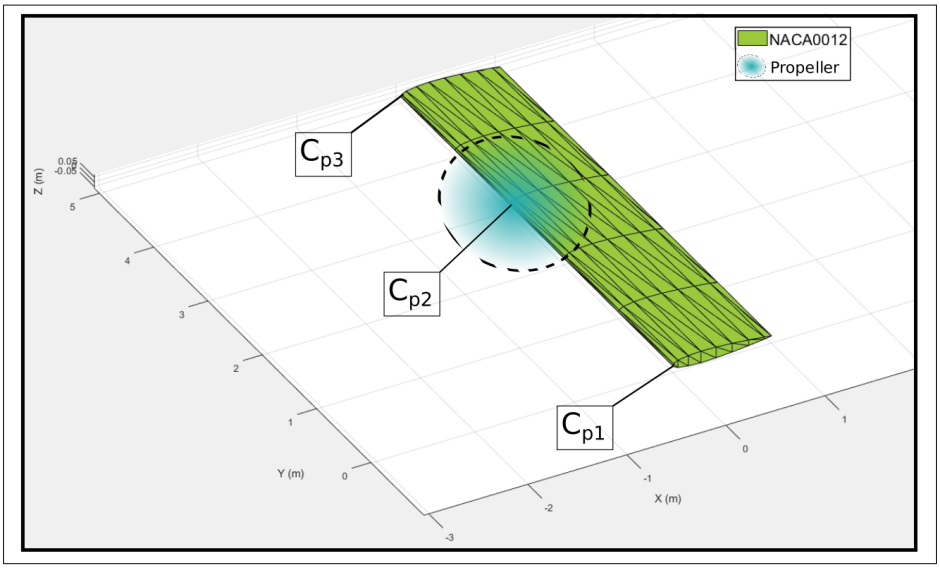

Figure 3.1 Pressure Coefficient Computation

(Figure 3.2) show the pressure distribution coefficient (C_p) on the root section of the wing obtained with the propeller slipstream.

(Figure 3.2) show the evolution evolution of the (C_p) with respect to the mesh used is obtained. The two different meshes having 18 and 100 chordwise and 5 panels spanwise. The comparison results along the NACA0012 wing with the two different meshes show that by increasing the number of panel element the pressure coefficient almost vanish at the tip section of the wing. Also, the resulting difference in the (C_p) values are due to the presence of the propeller in front

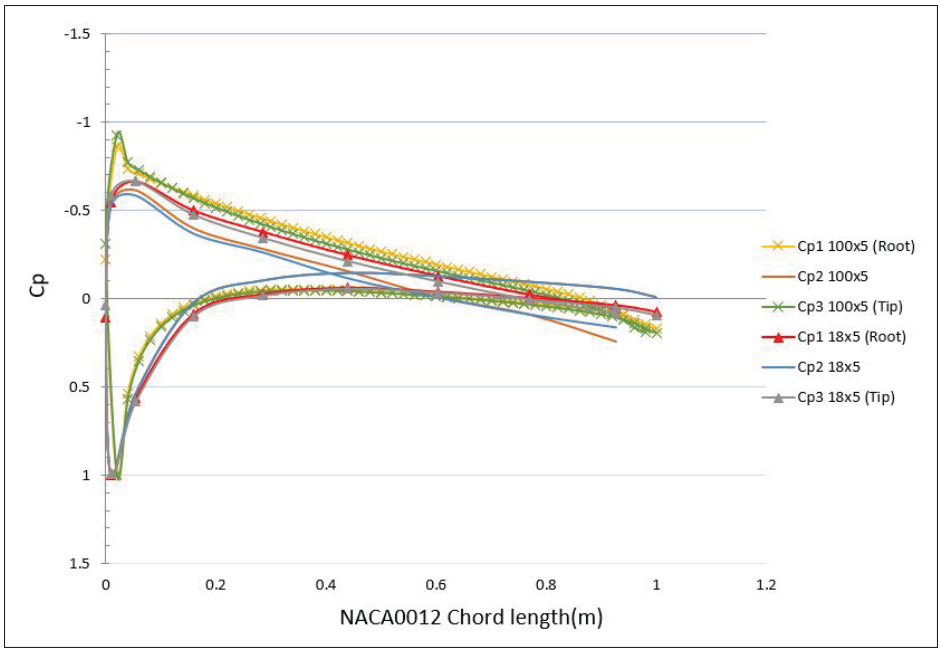

Figure 3.2 Pressure Coefficient Distribution on 3 Sections of the NACA0012 Airfoil

of the wing. The propeller produces additional energy along with the slipstream above the aircraft wing. These additional energy affect the velocity distribution above the wing equation (3.1-3.2) (Katz & Plotkin, 2001).

$$u = 2Q_\infty[\sin(\alpha+\beta) - \sin(\alpha-\theta)]\frac{a^4\cos\theta(A^2+B^2) + a^2\frac{c^2}{16}(B\cos\theta - A\sin\theta)}{(a^2A - \frac{c^2}{16})^2 + a^4B^2} \tag{3.1}$$

$$w = 2Q_\infty[\sin(\alpha+\beta) - \sin(\alpha-\theta)]\frac{a^4\cos\theta(A^2+B^2) - a^2\frac{c^2}{16}(B\sin\theta - A\cos\theta)}{(a^2A - \frac{c^2}{16})^2 + a^4B^2} \tag{3.2}$$

where (u, w) are the velocity distribution coordinates. The variation of the velocity distribution (u, w) affect the pressure coefficient (C_p) represented in equation (3.3) below from (Katz & Plotkin, 2001).

$$C_p = 1 - \frac{u^2 + w^2}{Q_\infty^2} \tag{3.3}$$

From this equation (3.3) can be recognized from the second term $1 - \frac{u^2+w^2}{Q_\infty^2}$ that the velocity distribution term increases due to this additional propeller energy. This additional energy produced by the propeller increases the velocity of the flow behind the propeller section. Also, the additional energy decreases the angle of attack which results a lower local lift area behind the propeller. In addition, the decrease of the angle of attack is due to the summation of the tangential induced velocity component in the y direction. Therefore, the summation of the tangential induced velocity component decreases the lift behind the propeller section. Therefore, the pressure coefficient (C_p) changes depending on the computation area on the airfoil root section.

3.2 Parametric Study

3.2.1 Ice Particle Geometrical Parameters Test Case Study

The ice shape fragments shed from the aircraft wing are random due to ice accretion. For simplification, the ice shape fragment is assumed to behave as a thin rectangular flat plate. Therefore, the ice particle is assumed to remain a flat plate when running all the test cases. The selection of the flat plate for this parametric study was kept from previous study of (El Sahely, 2019). This hypothesis is used according to other previous work from literature (Papadakis, Yeong, & Suares, 2007). Also, the rectangular flat plate hypothesis enables future comparison of the probability distribution function with (El Sahely, 2019).

This section is devoted to the geometrical parameters of the ice particle which influence

the trajectory. The single trajectory test cases will be performed for a NACA0012 airfoil. For each test case, all the ice particles will have the same initial velocity and initial orientation angle (Euler's angle). In addition, for every test case, the wing discretization is kept the same; eighteen panels chordwise and five panels spanwise (El Sahely, 2019). The selection of the discretization mesh (18x5) on NACA0012 used by (El Sahely, 2019) is based on:

- The NACA0012 airfoil panel discretization is similar to the one used by (Katz & Plotkin, 2001).
- The reduction of the ice trajectory computation time MATLAB code compared to other panel numbers.

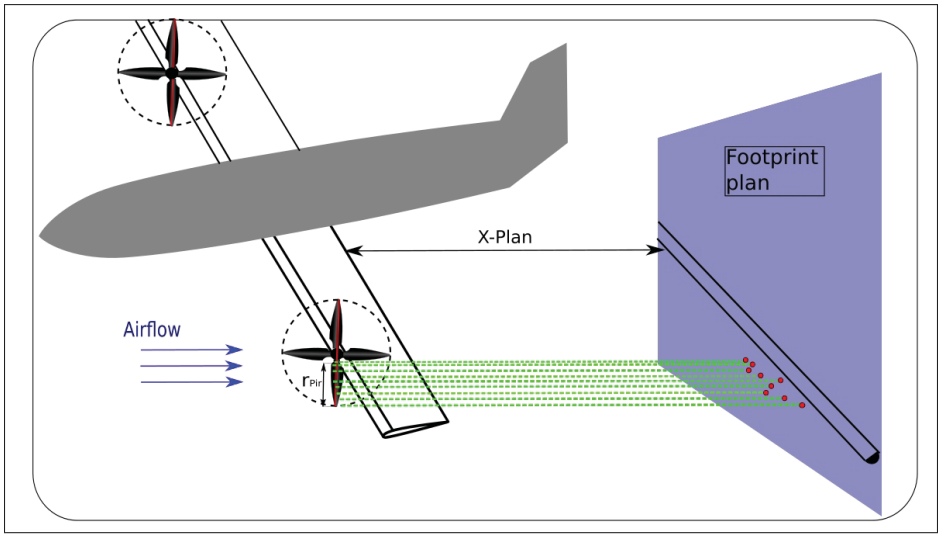

Figure 3.3 Sketch of the Ice Particle Shed with the Flowfield on the Aircraft Wing

(Figure 3.3) shows the sketch of the ice particle trajectory shed with the flowfield on the aircraft wing. The aircraft wing is based on a NACA0012 airfoil. X-Plan is the footprint map located at 6,5m behind the wing. (Figure 3.3) gives only an illustration of the ice trajectory study behind an aircraft wing with the propeller slipstream. From (Figure 3.3), it can be noticed that the trajectory footprint varies depending on the propeller inner radius r_{Pir}. Each propeller inner radius has a different value of induced velocity produced by the propeller. For, the parametric study and the PDF, the propeller blade radius is subdivided into 15 inner radiuses. Each inner

radius has its own axial and tangential induced velocities. The following two test cases will be performed by changing one geometrical parameter of the ice particle. Table (3.1) reveals the parameters for the single ice trajectory test cases study and it is subdivided into two rows:

- The first row has the initial parameters for the rectangular flat plate. Also, the wing geometrical initial parameters and the propeller geometrical parameters are given. These parameters are used in order to perform test cases (1-2).
- The second row has the variable parameters (THK) for test case number 1 shown in the first column and it is varied between $2cm$ and $15cm$. The variable parameter mass (m) for test case number 2 is shown as well in the second column and it is varied between $7.46g$ and $42.10g$. The variable parameter values are randomly selected for these parametric test case study.

Table 3.1 Initial and Variable Geometrical Parameters for Single Trajectory Test Cases 1&2

Test Case	**#1**	**#2**
Initial Parameters	Flat plate length $l = 21.22cm$ Plate width, $L = 10.61cm$ Plate surface ratio $SR = 2$ Flowfield velocity $V(t) = 113m/s$ Wing $AOA = 5°$ Propeller blade number $B = 4$ Propeller radius $R = 50cm$ Propeller rotational speed n=$2000RPM$ Altitude=$15000ft$ Wing half span $b = 5m$ Shed location $y = 2/5m$ Propeller location $y = 2/5m$ Axial induced velocity $V'_{ia_m} = 1.816 - 17.609m/s$ Tangential induced velocity $V'_{ia_t} = 1.561 - 6.246m/s$	
Variable parameter	Flat Plate thickness (THK) $2cm - 15cm$	Mass (m) $7.46g - 42.10g$

The first parametric study, designated as test case number 1, considers the variation of the ice particle (flat plate) thickness (THK) shown in (Figures 3.4-3.5-3.6). The calculation time for each trajectory is $0.8s$, with a timestep of $10ms$. (Figure 3.4) illustrates a single trajectory

shedding with different ice particle thickness around a NACA0012 wing (Y-Z) view. The NACA0012 wing is illustrated in green colour for this single ice trajectory computation. (Figure 3.5) illustrates the result of a single ice trajectory for test case number 1 in (Y-Z) view with a symmetry plane at $y = 0m$. The full-wing span is equal to $10m$; therefore, the illustration of a half-wing span is shown in green colour from $(0 - 5m)$. (Figure 3.6) shows the result of a single ice trajectory for test case number 1 in (X-Y) view.

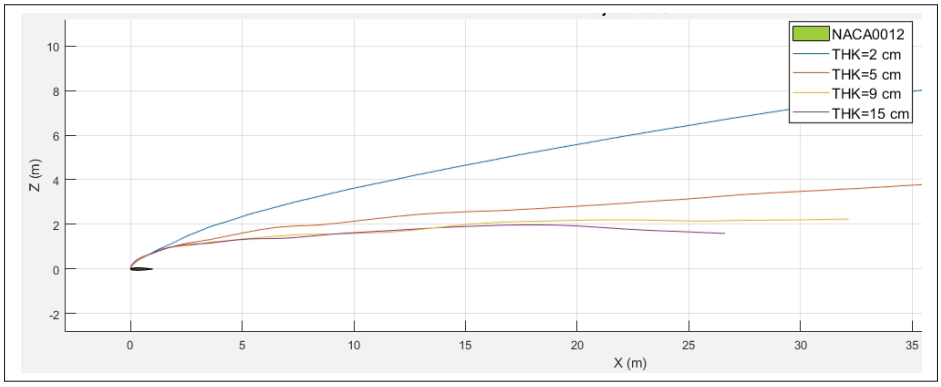

Figure 3.4 Test Case 1 : Single Trajectories with Different Ice Particle Thickness on a NACA0012 Airfoil (X-Z) View

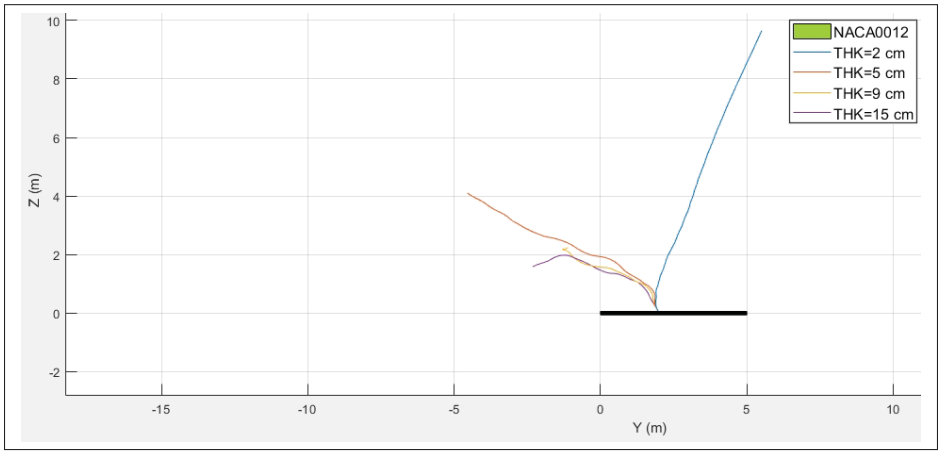

Figure 3.5 Test Case 1 : Single Trajectories with Different Ice Particle Thickness on a NACA0012 Airfoil (Y-Z) View

The second parametric test case study designated as test case number 2 will be based on changing the ice particle mass shown in (Figures 3.7-3.8-3.9) from the table (3.1) above. The calculation time for each trajectory is $0.8s$, with a timestep of $10ms$

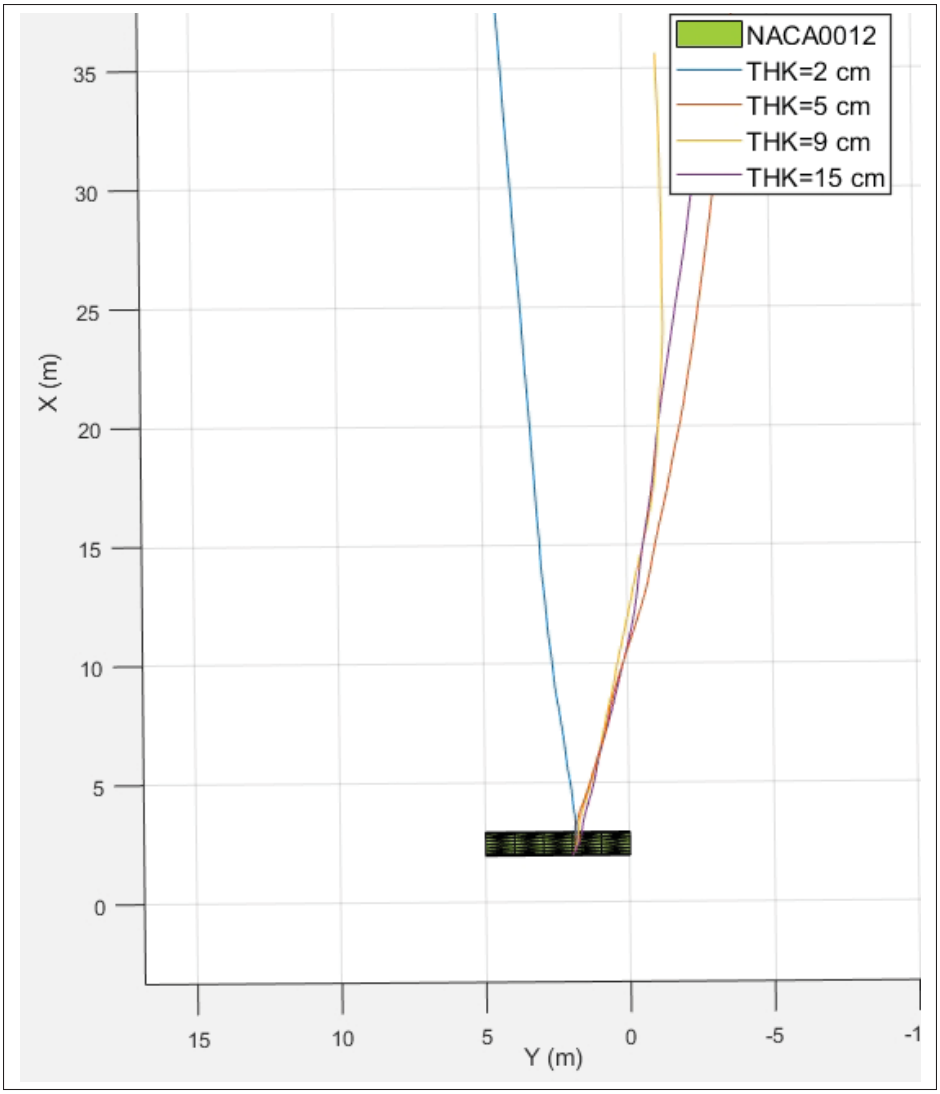

Figure 3.6 Test Case 1 : Single Trajectories with Different Ice Particle Thickness on a NACA0012 Airfoil (X-Y) View

From both test cases (1-2), it can be seen that by increasing one of the ice particle parameters (mass, thickness), the resultant obtained trajectory will fall toward the z-axis. This result is reasonable due to the increase of the ice particle weight which will tend to pull it more toward the x-axis.

Therefore, the ice particle thickness and mass will be considered as critical parameters due to their significant effect on the single ice trajectory. Besides that, the rest of the geometrical parameters of the ice particle was not studied.

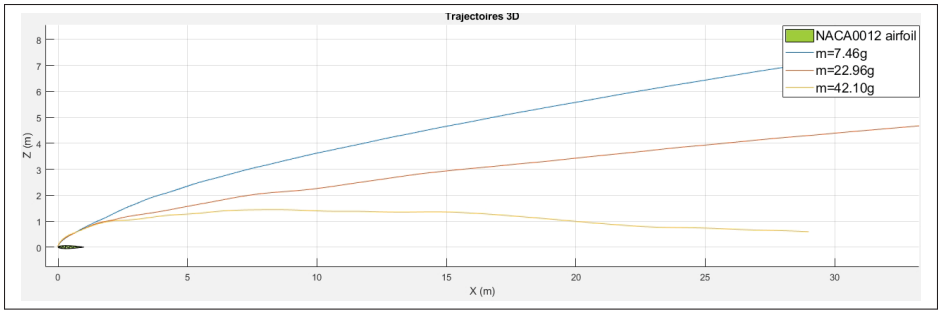

Figure 3.7 Test Case 2 : Single Trajectories with Different Ice Particle Weight on a NACA0012 Airfoil (X-Z) View

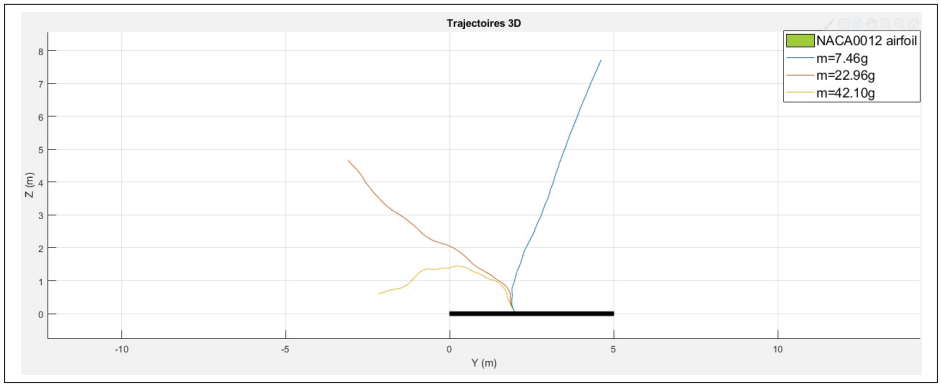

Figure 3.8 Test Case 2 : Single Trajectories with Different Ice Particle Weight on a NACA0012 Airfoil (Y-Z) View

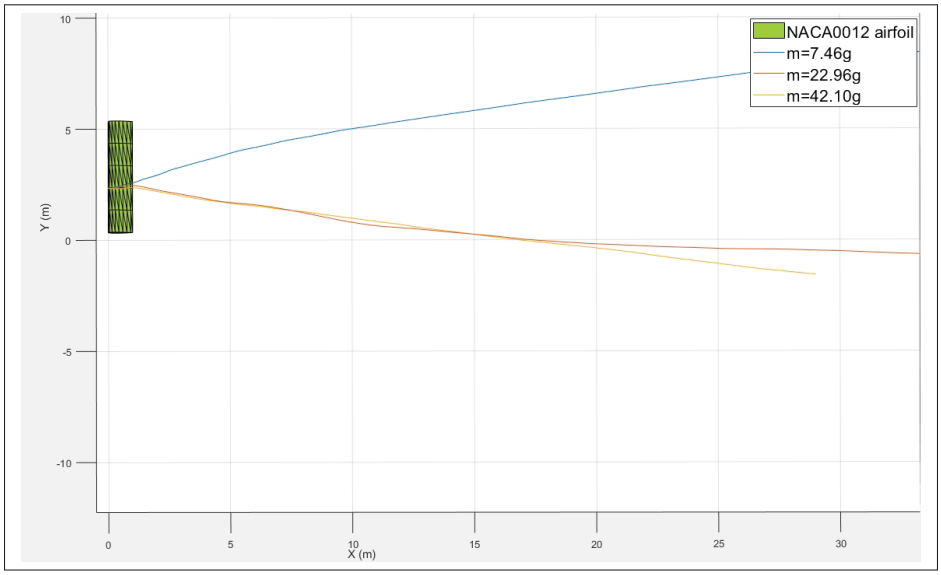

Figure 3.9 Test Case 2 : Single Trajectories with Different Ice Particle Weight on a NACA0012 Airfoil (X-Y) View

3.2.2 Aircraft Velocity Parameter Test Case Study

The effect of aircraft velocity on a single ice trajectory will be represented in this section. Therefore, the specific test case number 3 on the variable aircraft speed parameter will be performed. The test case number 3 intents to provide further verification on the effect of the slipstream produced by the propeller. The verification of the propeller slipstream effect will be done by decreasing the aircraft velocity, so that the slipstream effect will be more visible on the detached ice particle. (Table 3.2) shows the variable parameters for the test case number 3. It is necessary to point out that the initial parameters from (Table 3.1) were modified for this wing velocity parametric test study. Therefore, a new initial variable is added in (Table 3.2) and both values for ice particle mass and thickness are fixed.

Table 3.2 Initial and Variable Geometrical Parameters for Single Trajectory Test Case 3

Test Case	**#3**
Initial Parameters	Flat plate length $l = 21.22cm$ Plate width, $L = 10.61cm$ Plate surface ratio $SR = 2$ Propeller blade number $B = 4$ Propeller radius $R = 50cm$ Wing $AOA = 5°$ Mass $m = 7.7g$ Propeller rotational speed n=2000RPM Altitude=15000ft Flat Plate Thickness $(THK) = 2cm$ Wing half span $b = 5m$ Shed location $y = 2/5m$ Propeller location $y = 2/5m$ Axial induced velocity $V'_{ia_m} = 1.816 - 17.609m/s$ Tangential induced velocity $V'_{ia_t} = 1.561 - 6.246m/s$
Variable parameter	Flowfield velocity $V(t)$ 20 m/s - 60 m/s

(Figures 3.10-3.11-3.12) show the single ice particle shedding for the test case number 3 with different aircraft velocities $V(t)$. This test case doesn't consider the real aircraft velocity $V(t)$ values, since they are below stalling value and not suitable for flying operations. The purpose of

choosing these velocity magnitudes is so that the induced velocities produced by the propeller becomes more significant for the single ice trajectory shed. The calculation time for each trajectory is $0.8s$, with a timestep of $10ms$. From (Figure 3.10), for the value of $V(t) = 20m/s$, the trajectory length of the ice shed is 4 m. As well, for $V(t) = 40m/s$ the trajectory length obtained is 13 m. Therefore, when $V(t)$ increases, the ice shed trajectory length increases too. The increase in the ice trajectory shed length can have a greater effect on the surroundings of the aircraft wing. In addition to that, the variation of $V(t)$ changes the footprint map distance behind the flying aircraft. The slipstream effect can be observed on the lower velocity trajectories on (Figure 3.11). The slipstream effect is constant, therefore, it will be more significant at a lower flowfield velocity $V(t)$. In this case, the detached ice particles will sheds toward the right under the effect of the slipstream.

As a result, the effect of changing the aircraft velocity in test case number 3 is considered one of the critical parameters on the ice trajectories.

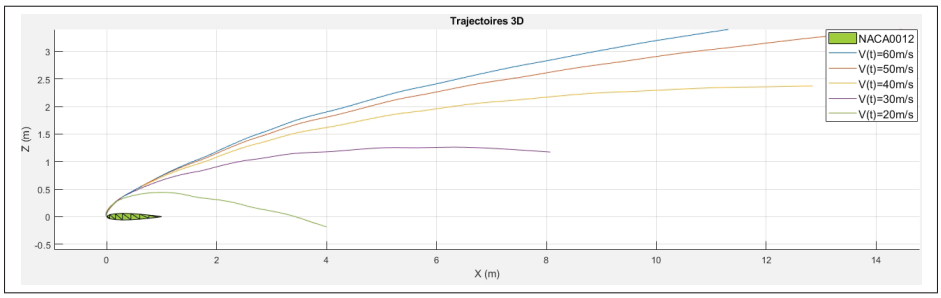

Figure 3.10 Test Case 3 : Single Trajectories on a NACA0012 Airfoil with a Different Aircraft Velocity (X-Z) View

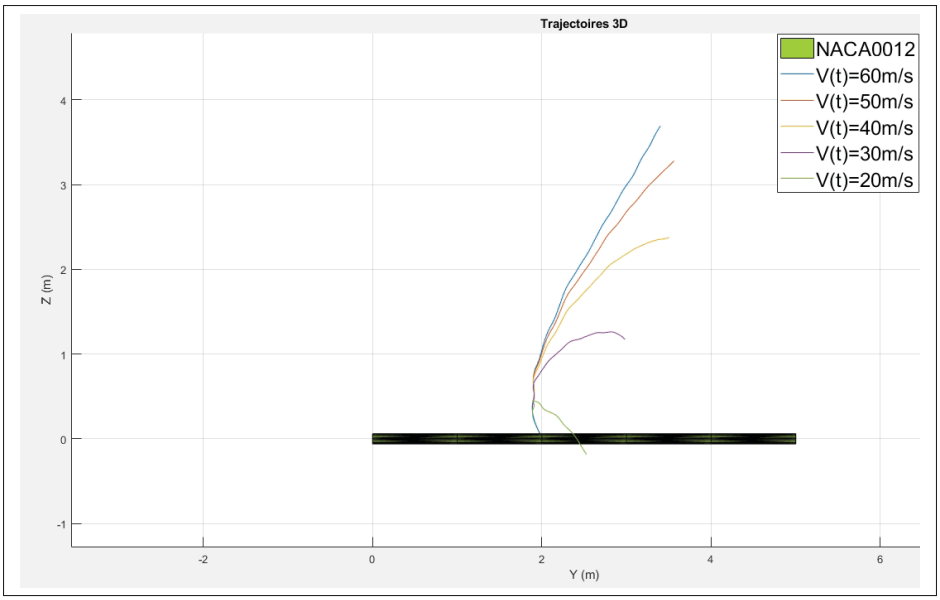

Figure 3.11 Test Case 3 : Single Trajectories on a NACA0012 Airfoil with a Different Aircraft Velocity (Y-Z) View

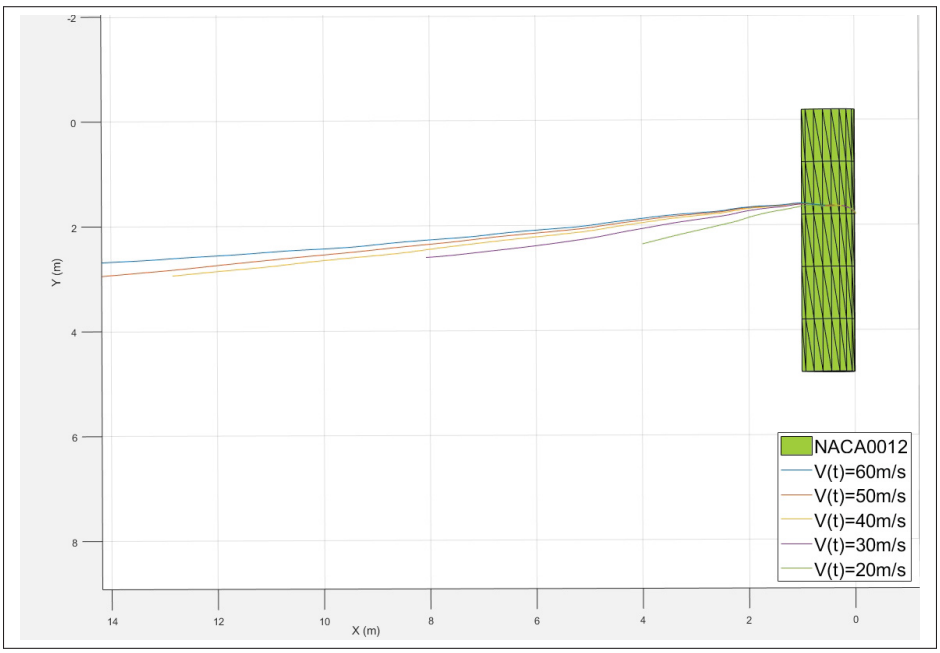

Figure 3.12 Test Case 3 : Single Trajectories on a NACA0012 Airfoil with a Different Aircraft Velocity (X-Y) View

3.2.3 Aircraft NACA0012 angle of attack test case study

The test case number 4 that follows is an example of the effect of changing the angle of attack (AOA) of the aircraft wing. This parametric test case study will use a single trajectory with initial and variable parameters shown in the table (3.3). Also, a modification of the aircraft velocity compared to table(3.1) will be made by decreasing it to 50 m/s. Again, this aircraft $V(t)$ is not suitable for flying operation. This modification is made so that the slipstream becomes more significant in the shed ice trajectory. Therefore, the behaviour of the angle of attack might be more effective on the shed ice particle.

Table 3.3 Initial and Variable Geometrical Parameters for Single Trajectory Test Case 4

Test Case	**#4**
Initial Parameters	Flat plate length $l = 21.22cm$ Plate width, $L = 10.61cm$ Plate surface ratio $SR = 2$ Flowfield velocity $V(t) = 50m/s$ Propeller blade number = 4 Propeller radius $R = 50cm$ Mass $m = 7.7g$ Propeller rotational speed=2000RPM Altitude=15000ft Flat Plate Thickness $(THK) = 2cm$ Wing half span $b = 5m$ Shed location $y = 2/5m$ Propeller location $y = 2/5m$ Axial induced velocity $V'_{ia_m} = 1.816 - 17.609m/s$ Tangential induced velocity $V'_{ia_t} = 1.561 - 6.246m/s$
Variable parameter	Wing AOA $0 - 15°$

The results of the test case number 4 are shown in the (Figure 3.13-3.14-3.15) with different angles of attack (AOA). From the (Figure 3.13), it can be seen that for the angle of attack ($AOA = 0°$), the ice trajectory shed has reached a height of 4,5 m above the wing. The result obtained for a greater value of ($AOA = 10°$) shed the ice particle on a higher height which is 9 m. The same effect is observed for ($AOA = 15°$) where the shed height increases to 13 m.

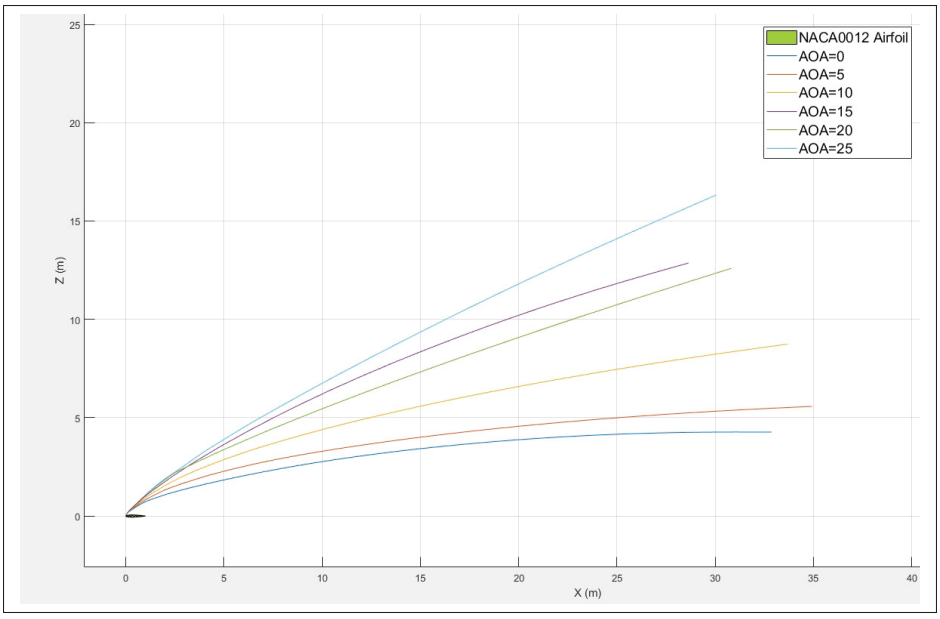

Figure 3.13 Test Case 4 : Single Trajectories on a NACA0012 Airfoil with a Different AOA (X-Z) View

However, inspection of the ice trajectory shed result for AOA above 15° is not considered: ice trajectory obtained for ($AOA = 20° \rightarrow 25°$) are rejected in this study due to PM limitations. The PM cannot predict the flowfield separation at the stalling angle. Also, because the flow is considered to be steady, another PM limitation for analyzing angle above stalling is added. Therefore, the effect of changing the aircraft angle of attack in test case number 4 is considered one of the critical parameters on the ice trajectories.

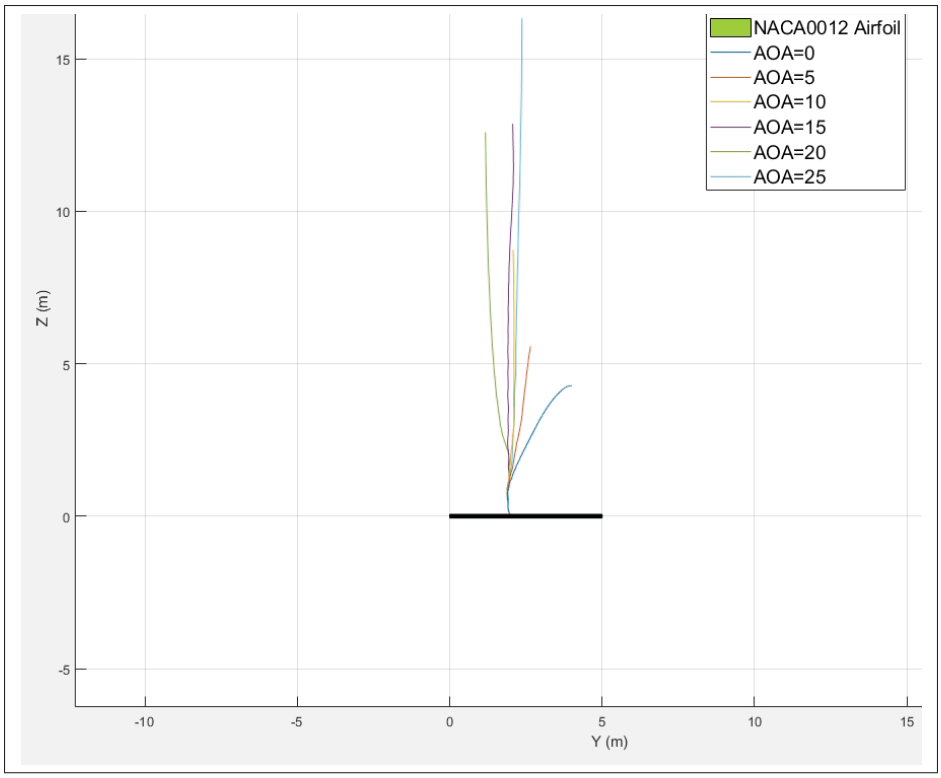

Figure 3.14 Test Case 4 : Single Trajectories on a NACA0012 Airfoil with a Different AOA (Y-Z) View

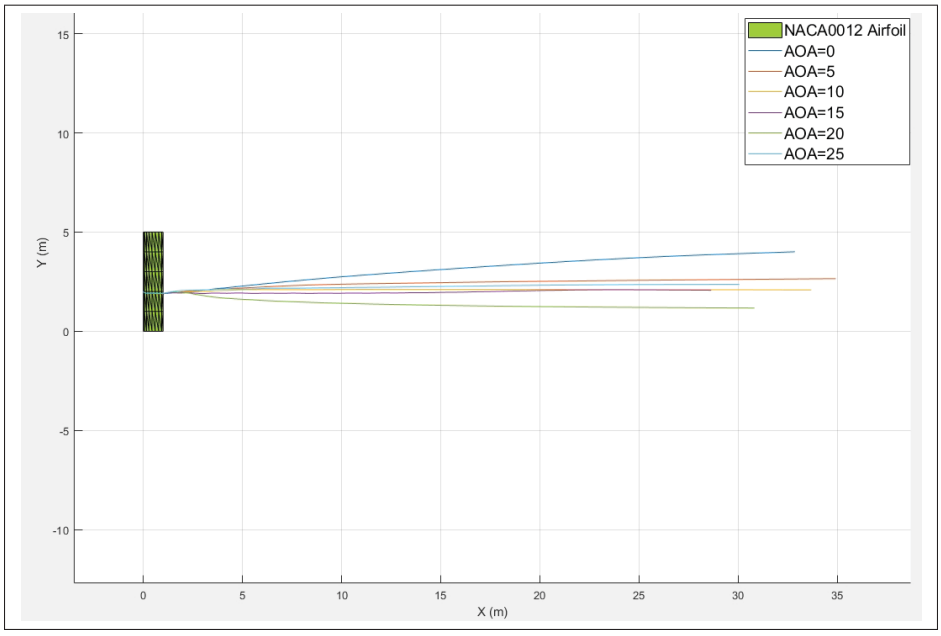

Figure 3.15 Test Case 4 : Single Trajectories on a NACA0012 Airfoil with a Different AOA (X-Y) View

3.2.4 Propeller geometrical parameters test case study

The following section will describe the effect of the propeller geometrical parameter. From the previous parametric study made by (Dimchev, 2012), it was shown that the increase of the propeller blade number has a direct effect on the swirl produced by the propeller. Therefore, a specific test case number 5 on the variable propeller blade number parameter will be performed. It intends to verify the effect of the slipstream produced by the propeller. In addition, a parametric study on the size of the propeller will be executed to see its impact on the single ice particle trajectory designated under test case number 6. (Table 3.4) shows the initial and variable parameters including both values for the propeller blade numbers and the propeller radius for both test cases (5-6).

Table 3.4 Initial and Variable Geometrical Parameters for Single Trajectory Test Cases 5&6

Test Case	**#5**	**#6**
Initial Parameters	Flat plate length $l = 21.22cm$ Plate width, $L = 10.61cm$ Plate surface ratio $SR = 2$ Flowfield velocity $V(t) = 50m/s$ Wing $AOA = 5°$ Mass $m = 7.7g$ Propeller rotational speed=2000RPM Altitude=15000ft Flat Plate Thickness $(THK) = 2cm$ Wing half span $b = 5m$ Shed location $y = 2/5m$ Propeller location $y = 2/5m$ Axial induced velocity $V'_{ia_m} = 1.816 - 17.609m/s$ Tangential induced velocity $V'_{ia_t} = 1.561 - 6.246m/s$	
Variable parameter	Propeller blade number (n) $2 - 6$	Propeller radius R $50 - 200$

The results from test case number 5 shows that by increasing the propeller blade number, the propeller normal force coefficient increases too. Moreover, no variations for both the axial and tangential velocities are observed, which does lead to a zero-difference ice trajectory on the NACA0012 wing. In addition, the result of test case number 6 shows an unaffected ice particle

trajectory or zero difference. The propeller parametric study was important to prove that neither of these modifications on the propeller radius or propeller blade number will affect the detached flight ice particle.

3.3 Three-dimensional Probability Distribution Function (3DPDF)

One of the important tools for the trajectory study is the probability distribution function (PDF). The following section will perform a three-dimensional probability distribution function study (3DPDF). This (3DPDF) will allow spotting the area where the probability of ice passage is higher around the aircraft wing. This area is the one impacted by the dismantled flying ice particles. The 3DPDF of 1000 trajectories is chosen in this study, this number of trajectories is the same one used by (El Sahely, 2019). The choice of 1000 is based on the fact that the PDF of the trajectory remains almost the same after this number of trajectory simulation. This was demonstrated by (El Sahely, 2019).

Also, in order to compare the obtained results with the (3DPDF) made by (El Sahely, 2019), each trajectory obtained in this simulation comes from the release of the ice particle in the space for one second with a time step of 1×10^{-3} second.

(Figure 3.16) illustrates the 3D view of 1000 trajectories behind the aircraft wing. (Figure 3.16) was obtained at the angle of attack equal to $AOA = 5°$ and sweep back angle equal SBA= 0 with flowfield velocity= $113m/s$. The wing has a half-wing span of 5 m presented in black. The ice particle is located at $y = 3m$ of the airfoil and the footprint map is at $6.5m$.

Table(3.5) shows the initial parameters used for the two following trajectory simulations. From Table (3.5), it can be observed that the two simulations have been performed for 1000 ice trajectories. Table (3.5) describes the propeller and slipstream characteristics used for this simulation.

Two simulations are performed with different flowfield velocities to better visualize the effect of the slipstream produced by the propeller. The visualization will be shown later by comparing the ice trajectories footprints depending on the flowfield given. The first simulation shown in the table (3.5) is performed with the flowfield velocity surrounding the aircraft equal to 113 m/s.

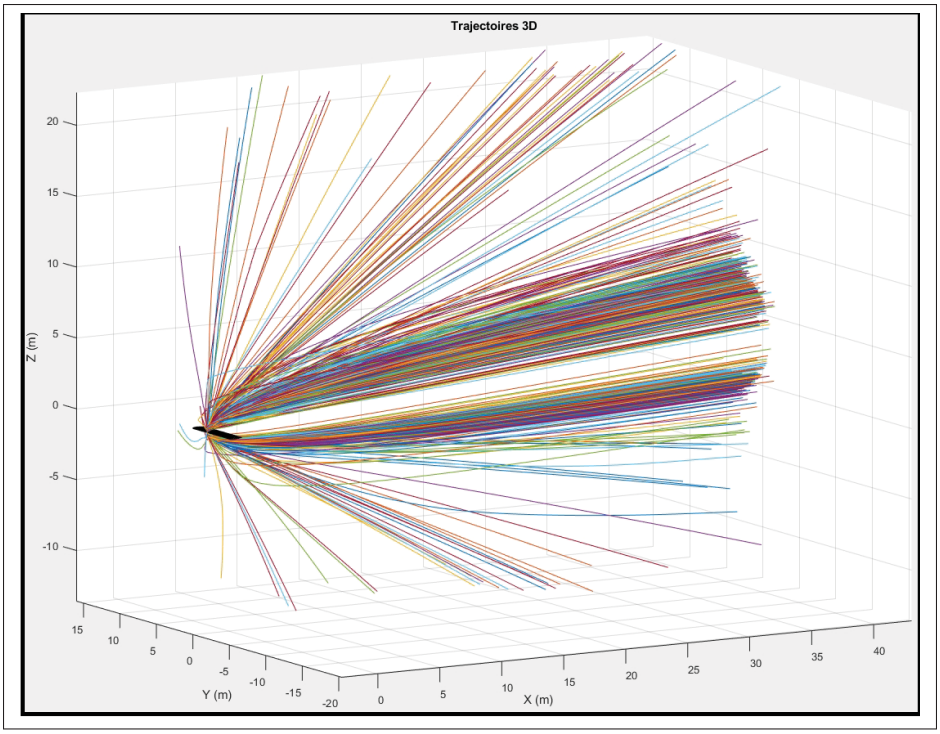

Figure 3.16 3D View of 1000 Ice Trajectories at $AOA = 5°$ with $V(t) = 113m/s$

The second simulation is performed with a flowfield velocity surrounding the aircraft equal to 30 m/s.

The slipstream induced velocities were obtained previously from chapter 2 using the (Vel_conv) MATLAB function. This MATLAB function determines the induced velocities produced by the propeller over the wing section. For the two performed simulations (1-2), the wing and flat plate characteristics are kept similar (El Sahely, 2019). In addition to that, the fat plate rectangular shape doesn't change during both trajectory simulation (1-2). (Figure 3.16) shows the 3D view of 1000 ice trajectories from the first simulation with V(t)=113 m/s. This (Figure 3.16) serves only as an illustration of the capability of TRAJPM in obtaining the simulation of a flying ice particle.

It is important to mention that a comparison of a 3D scheme is a very difficult task. Therefore, the following simplification for the PDF comparison will be made by using the MATLAB

Table 3.5 Characteristics of the Initial Parameters for 1000 Trajectories Simulations

Simulation Number	1	2
Number of simulated trajectories N	1000	1000
Flowfield Velocity $V(t)$	$113m/s$	$30m/s$
Wing characteristics	Type of airfoil= NACA0012 Aspect ratio= 5 Panel discretization=18x5 SBA= 0 AOA=5° Chord length $c = 1m$ Wing half span $b = 5m$ Shed location $y = 3/5m$ Propeller location $y = 3/5m$ Root Chord $C_R = 1m$ Tip chord $C_t = 10m$	
Propeller characteristics	Number of propeller blades $B = 4$ Propeller location from root section= $3m$ Propeller radius $R = 70cm$ Propeller revolution per minute (RPM) $n = 2000$	
Flat plate characteristics	Mass of the flat plate $m = 7.7g$ Flat plate dimension= $0.2122m$x$0.1061m$x$0.002m$ Plate surface ratio $SR = 2$ Intel Euler's angle= $[20, 30, 20]$ Plate thickness THK= $0.002m$ Shed location from root section= $3m$	
Slipstream characteristics	Altitude=$15000ft$ Gravitional force g= $9.671m/s^2$ Air density $\rho = 0.77(kg/m^3)$ Axial induced velocity $V'_{ia_m} = 1.816 - 17.609m/s$ Tangential induced velocity $V'_{ia_t} = 1.561 - 6.246m/s$	

function made by (El Sahely, 2019) which depicts the 3D view of P(Y, Z). This MATLAB function allows creating two projections. The first one is P(Y), the projection on (Y-axis). It shows the probability distribution (PDF) of the trajectory footprint on (Y-axis). The second one is P (Z), the projection on (Z-axis). It shows the PDF on (Z-axis) of the trajectory footprint. The assumption of a binormal distribution will be confirmed later for P(Y) and P(Z).

(Figure 3.17) shows the back view of a flying aircraft with the ice trajectories footprint map.

This footprint map is situated from 6.5 m downstream behind the aircraft wing for both trajectory simulations (1-2). (Figure 3.17) shows the ice particle shed above and below the aircraft wing as a footprint map. Not all 1000 trajectories are displayed in this footprint map (Figure 3.17) since some of these dismantled ice particles have collided with the wing.

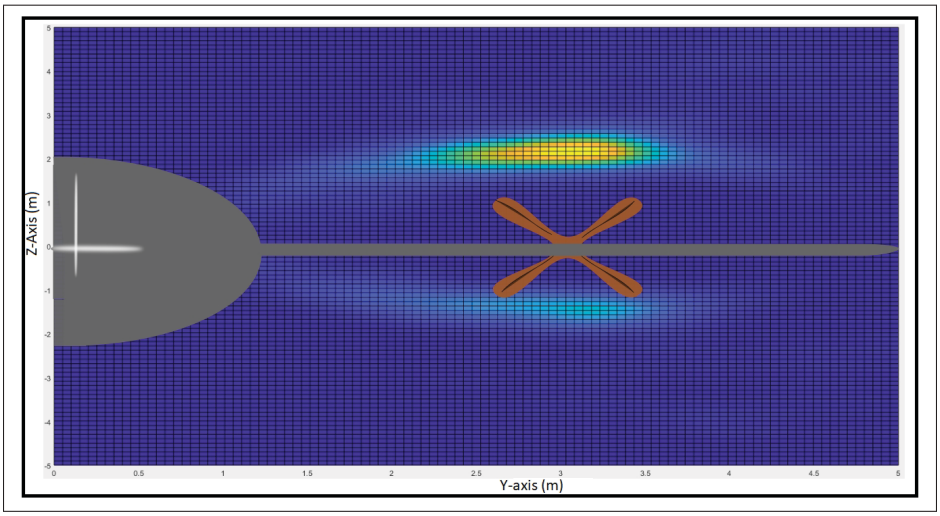

Figure 3.17 Simulation 1 : Probability Distribution of the Footprint Trajectories for 1000 Trajectories Along X and Y-axis with $V(t) = 113m/s$

(Figure 3.18) shows the PDF of the trajectory's footprint with respect to the Y-axis for the simulation number 1 done with 1000 trajectories. The variation of the PDF for these trajectories is more visible with the help of (Figure 3.17). Starting from 0 m on (Y-axis) and moving from left to right till 5 m, the yellow area can be detected upside the wing. This yellow area is mostly between y=2.5m and y=3.5 m which corresponds to the same result outcome from (Figure 3.18). Also, (Figure 3.18) shows a probability of ice passage equal to 57% above the wing in this area (2.5m-3.5m). The rest of the ice particle shed is distributed along the wing span (grey colour) and can be observed in light blue and green in (Figure 3.17). In addition, a comparison of the PDF between simulation number 1 and the one achieved by (El Sahely, 2019) in (Figure 3.17), shows that both curves have a similar tendency. Moreover, there is a higher concentration on the Y-axis for simulation number 1 designated as (Prop+Wing) in (Figure 3.17). The higher concentration attained is due to the presence of the slipstream produced by the propeller placed

in front of the aircraft wing. Therefore, a higher concentration of the footprint map behind the propeller area above the wing is created. The shape of this PDF is a normal distribution analogous to (El Sahely, 2019).

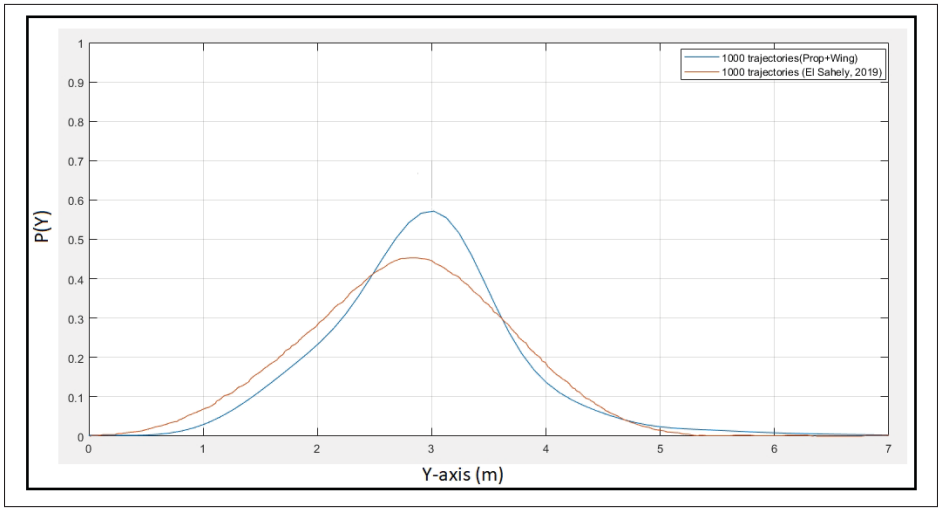

Figure 3.18 Simulation 1 : Probability Distribution of the Trajectory's Footprint with Respect to the Y-axis with $V(t) = 113m/s$

(Figure 3.19) represents the PDF of the trajectory's footprint with respect to the Z-axis. In order to analyze it, another examination of (Figure 3.17) will be helpful. By reviewing the Z-axis in (Figure 3.17) starting from the bottom part $z = -4m$ till $z = 5m$, it can be seen that there are two concentrated areas. The first concentrated area is the one below the wing between $z = -2m$ and $z = -0.5m$. The first concentration area is in light blue since it only represents 27% of the footprint concentration below the wing. The second concentrated area is between z=1.5m and z=3m above the wing. The second concentration area is in yellow since it does show 60% of the footprint concentration above the wing. Moreover, a comparison of the PDF between simulation number 1 and the one achieved by (El Sahely, 2019) in (Figure 3.19) shows a higher concentration on the Z-axis for simulation number 1 designated as (Prop+Wing) in (Figure 3.19). Also, the comparison reveals that both curves have the same tendencies along the Z-axis and binormal distribution. Both projections on P(Y) and P(Z) for P(r) give a higher concentration area for the propeller with wings using the same V(t).

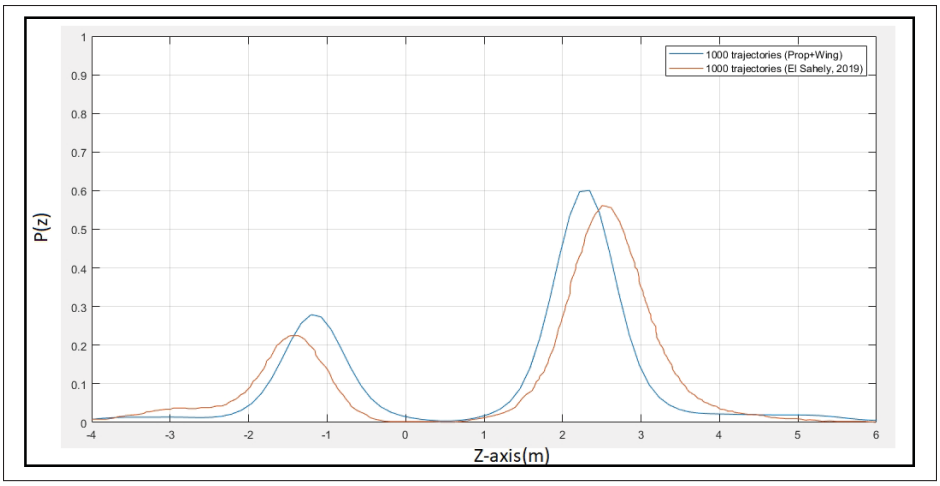

Figure 3.19 Simulation 2 : Probability Distribution of the Trajectory's Footprint with Respect to the Z-axis with $V(t) = 113m/s$

This master thesis aims to visualize the propeller effect on the ice shed trajectory. Therefore, in order to visualize more the slipstream effect produced by the propeller simulation number 2 is done. This simulation number 2 is done with a V(t)=30 m/s so that the slipstream velocities over the wing become more significant on the flow. (Figure 3.20) shows the 1000-trajectory footprint map from the back view of an aircraft wing resulted from simulations number 2.

This simulation number 2 will serve to see if the PDF is concentrated more in some areas due to significant induced velocities over the aircraft wing. (Figure 3.21) shows the probability distribution of the trajectory's footprint with respect to the Y-axis for the simulation number 2. The changes of this PDF on each section of the aircraft wing for these trajectories are more visible with the help of (Figure 3.20). Starting from 0 m on (Y-axis) and moving from left to right till 5 m, the yellow area can be detected upside the wing. This yellow area is mostly between y=2.5m and y=3.5 m which corresponds to the same result outcome from (Figure 3.21). Also (Figure 3.21), gives a probability of 54% of the shed ice particle above the wing in this area (2.5m-3.5m). In addition, the probability on the P(Y) from simulations number 1 and the P(Y) achieved by (El Sahely, 2019) have been fitted. This fitment is made to show that the projection on (Y-axis) has achieved the same tendency and giving a normal distribution. Also,

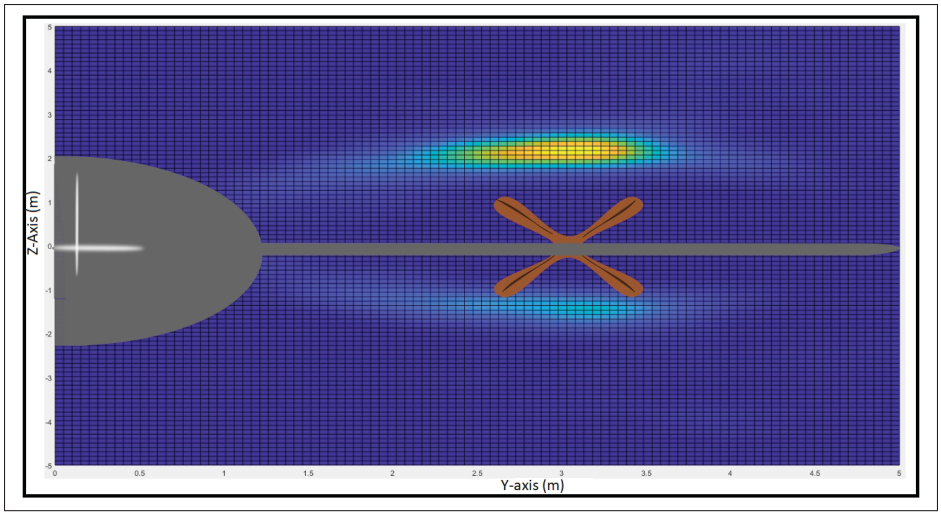

Figure 3.20 Simulation 2 : Probability Distribution of the Footprint Trajectories for 1000 Trajectories Along X and Y-axis with $V(t) = 30m/s$

the result shows that simulations number 2 have a less concentrated area above the wing than simulation number 1 on the (Y-axis). Nevertheless, the result outcome from simulations number 2 is still giving a higher concentration than the one obtained from (El Sahely, 2019), which can be explained by the slipstream effect.

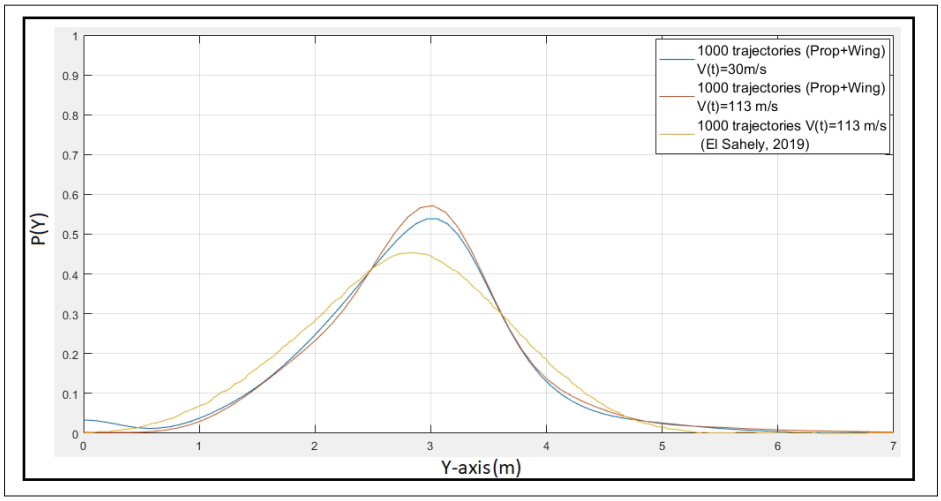

Figure 3.21 Simulation 2 : Probability Distribution of the Trajectory's Footprint with Respect to the Y-axis with $V(t) = 30m/s$

After observing the probability managed from simulations number 2 and the result of the trajectory footprint along the wing, another projection on (Z-axis) is done. This projection will serve to observe in case of a higher concentrated area being formed from simulations number 2. (Figure 3.22) show the probability distribution of the trajectory's footprint with respect to the (Z-axis) from simulations number 2. From this (Figure 3.22), it can be seen that the curves resulted from the projection on (Z-axis) have the same tendency and binormal distribution similar to (El Sahely, 2019) and simulation number 1. By reviewing the Z-axis in (Figure 3.22) starting from the bottom part $z = -4m$ till $z = 5m$, it can be seen that there are two concentrated areas. The first concentrated area is the one below the wing between $z = -2m$ and $z = -0.5m$. The first concentration area is in light blue since it only represents 26% of footprint concentration below the wing. The second concentrated area is between $z = 1.5m$ and $z = 3m$ above the wing. The second concentration area is in yellow since it does show 58% of footprint concentration above the wing.

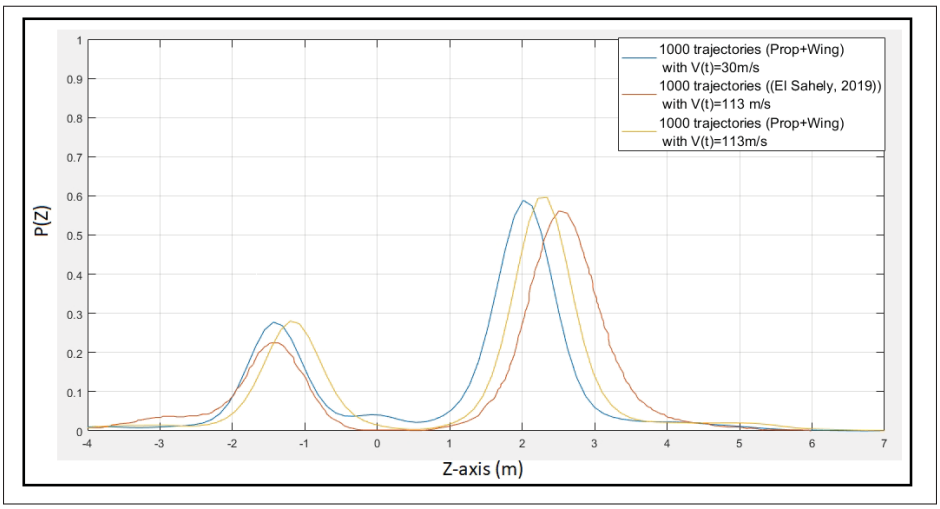

Figure 3.22 Simulation 2 : Probability Distribution of the Trajectory's Footprint with Respect to the Z-axis with $V(t) = 30m/s$

The probability distribution on the (Z-axis) result formed from simulations number 2 gave a lower concentration area than simulation number 1. Nevertheless, the slip stream effect over the wing is present and can be seen by the higher distribution obtained from (El Sahely, 2019).

CONCLUSION AND RECOMMENDATIONS

Ice accretion is one of the main potential hazards which lead to aircraft aerodynamic stall. Also, ice accretion on the aircraft components can result in a temporary loss of control during flight. Various deicing and anti-icing systems can be installed on the aircraft frame. These deicing systems main task is to prevent the formation of large ice layers on the aircraft components during flight operation. Since the integration of these decing systems, a new problem has been generated which is the unknown detached ice particle trajectory. The accreted ice particle dismantled from the aircraft wing follows a trajectory which can strike the surrounding aircraft components. This one can affect the safety of the aircraft structure. This research focused on the ice particle trajectories behind the propeller slipstream. The ice particle behind the slipstream is dismantled with an additional induced velocity produced by the propeller. A numerical approach is used to study these unknown trajectories behind the propeller slipstream. Also, an ice particles footprint map study is employed to evaluate the risk of its impact with the surrounding aircraft components. The aim of this research is to quantify the propeller slipstream effect on the ice shed trajectory.

The first objective was to propose a model that can study the propeller induced velocities on the wing for the ice trajectory simulation. A 3DPM solver is used to compute the flowfield around the aircraft wing like (El Sahely,2019). As well, a combination of the 3DPM with Qprop advanced BEMT is used to compute the flow behind the propeller slipstream. The Qprop tool is used similarly as (Dimchev, 2012) for this trajectory code. The method of implementation of the propeller induced velocity is presented in chapter 2. Qprop provides the induced velocities from the propeller plane. A methodology proposed by (Stone,2008) is used to determine the axial and tangential induced velocities over the wing due to the slipstream contraction over the wing. This implementation has granted a higher accurate flowfield for the wing element. The flowfield solution was obtained from the 3DPM combined with Qprop.

The second objective was to verify the flowfield of the built tool. Therefore, a pressure coefficient distribution study is conducted on the root section of the wing with a panel configuration of (18 × 5). The results of the pressure distribution computation showed that the value of C_{p2} change in the mid-section of the wing behind the propeller slipstream. Besides that,(C_{p1}, C_{p3}) remain almost the same as the flow without propeller at the tip and root section of the wing. This result verifies the slipstream effect on the pressure coefficient distribution. In addition, a lower local lift is obtained behind the propeller slipstream compared to the root and tip of the wing.

The third objective was to conduct a parametric study on a single ice particle shed. The parametric study was done in order to observe the effect of the slipstream on the detached ice particle. This shed ice particle was located at Y=3m on the wing behind the propeller slipstream. This parametric study looks at the effect of changing a single variable from the initial shed. From test case (1–2), the results showed that the increase in ice particle mass and thickness will pull the shed trajectory toward the gravity direction. The behaviour of the trajectory is due to the increase of the gravitational force on the shed ice particle. From test case (3), the result showed that the increase in the flowfield velocity does increase the shed ice particle trajectory length. From test case 4, the result showed that the increase of AOA does increase the length of the shed ice particle trajectory. This result is only valid for the angle of attack below 17 degrees due to 3DPM trajectory code limitations. From test case (5–6), the results show that the variation of the propeller parameter gives a zero difference in the shed ice particle trajectory.

The fourth objective determined the PDF footprints on the first simulation for 1000 trajectories by assuming the shape of PDF. To simplify the task of the 3DPDF comparison, two projections are made on Y and Z axis similar to (El Sahely,2019). Also, the probability shape assumption was kept the same normal on P(Y) and binormal on $P(Z)$. In addition, the fourth

objective was to compare the obtained PDF from simulation number 1 with one without the effect of the propeller slipstream (El Sahely,2019). The result of the comparison gave a higher probability of ice passage than the one obtained from (El Sahely, 2019) on P(Y). This result was seen on the P(Y) between (2.5m-3.5m) and showed a value of 57% compared to 45% attained by (El Sahely,2019). A similar effect is seen on the binormal distribution $P(Z)$ and gave two higher concentrated areas. The comparison of the first concentrated area between z(-2 m, -0.5 m) has shown 27% probability of ice passage below the wing compared to 22% achieved by (El Sahely,2019). Also, the comparison of the second concentrated area between z(1.5 m, 3 m) revealed 60% probability of ice passage compared to 56% obtained by (El Sahely,2019). Therefore, it can be concluded that the propeller slipstream has an effect on the probability of ice passage due to the observed higher concentration area.

The fifth objective focused on the second simulation for 1000 trajectories which was made to quantify further the slipstream effect. The methodology is based on decreasing the flow velocity to 30 m/s. This modification gave a lower flow field velocity so that the slipstream significance is higher on the shed ice trajectories. The result of ice passage obtained is almost similar to the first simulation on $P(Y)$ and $P(Z)$. Nevertheless, a critical observation is made on $P(Y)$ and $P(Z)$. By making the slipstream more significant, the probability of ice passage appears toward the fuselage. The PDF obtained on $P(Y)$ and $P(Z)$ showed some ice footprints near the fuselage area. This can have a potential impact on the aircraft structure.

Some recommendations for future improvements of the tool can be listed below:

- The first improvement can be to investigate the probability of the shed ice regarding where they impact onto the aircraft components.
- The second improvement is the integration of the prop-fan engine which has the contra-rotating fan arrangement to quantify the slipstream effect on the ice trajectory.

- The third recommendation is to consider that the ice particle is located on the propeller blade during rotation, adding a rotational velocity at the start of the trajectory calculation.

BIBLIOGRAPHY

Addy Jr, H. E., Broeren, A. P., Potapczuk, M. G., Lee, S., Guffond, D., Montreuil, E. & Moens, F. Ice accretions and full-scale iced aerodynamic performance data for a two-dimensional NACA 23012 airfoil. *SAE Technical report*.

Aref, P., Ghoreyshi, M., Jirasek, A., Satchell, M. J. & Bergeron, K. (2018). Computational study of propeller–wing aerodynamic interaction. *Aerospace*, 5(3), 79.

Baruzzi, G. S., Lagacé, P., Aubé, M. S. & Habashi, W. G. (2007). Development of a Shed-ice Trajectory Simulation in FENSAP-ICE. *SAE Technical Paper*.

Cao, Y., Ma, C., Zhang, Q. & Sheridan, J. (2012). Numerical simulation of ice accretions on an aircraft wing. *Aerospace Science and Technology*, 23(1), 296-304. doi: https://doi.org/10.1016/j.ast.2011.08.004.

Castro Santos, L., Papa, R. & Ferrari, M. D. A. (2003). A Simulation Model for Ice Impact Risk Evaluation. *41st Aerospace Sciences Meeting and Exhibit*, pp. 30.

Cavainolo, B. A. (2020). Development of a Computationally Inexpensive Method Of Simulating Primary Droplet Breakup. *SAE Technical report*.

Currie, T. C., Fuleki, D., Knezevici, D. C. & MacLeod, J. D. (2013). *Altitude scaling of ice crystal accretion*. Conference Proceedings presented in 5th AIAA Atmospheric and Space Environments Conference.

Dimchev, M. (2012). *Experimental and numerical study on wingtip mounted propellers for low aspect ratio UAV design*. (Thesis, Delft University of Technology).

Drela, M. (2007). QPROP user guide. *Massachusetts Inst. of Technology Aeronautics and Astronautics, Cambridge, MA (SAE Technical report)*.

Droandi, G. & Gibertini, G. (2012). Assessment of a Propeller Model Embedded on a Panel Method Code for Aircraft Aerodynamics. *Aerotecnica Missili & Spazio*, 91, 98-108.

El Sahely, H. (2019). *Study of the trajectories of ice shed by deicing system around aircraft engine*. (Thesis, École de technologie supérieure).

Favier, D., Ettaouil, A. & Maresca, C. (1989). Numerical and experimental investigation of isolated propeller wakesin axial flight. *Journal of Aircraft*, 26(9), 837-846. doi: 10.2514/3.45849.

Filburn, T. (2020). Anti-ice and Deice Systems for Wings, Nacelles, and Instruments. In *Commercial Aviation in the Jet Era and the Systems that Make it Possible* (pp. 99-109). Springer.

Gamme, S., De Oliveira Andrade, G., Ragni, D. & Lau, F. (2017). *A Fast Panel Code for Complex Actuator Disk Flows*. doi: 10.2514/6.2017-0752.

Glauert, H. (1935). Airplane Propellers. In *Aerodynamic Theory: A General Review of Progress Under a Grant of the Guggenheim Fund for the Promotion of Aeronautics* (pp. 169-360). Berlin, Heidelberg: Springer Berlin Heidelberg. doi: 10.1007/978-3-642-91487-4_3.

Goldstein, S. (1929). On the vortex theory of screw propellers. *Proceedings of the Royal Society of London. Series A, Containing Papers of a Mathematical and Physical Character*, 123(792), 440-465.

Hess, J. L. (1974). The problem of three-dimensional lifting potential flow and its solution by means of surface singularity distribution. *Computer Methods in Applied Mechanics and Engineering*, 4(3), 283-319.

Higham,Desmond & J Higham, N. J. (2016). MATLAB guide second edition (vol. 150). Society for Industrial and Applied Mathematics.

Horák, V., Rozehnal, D., Chára, Z. & Hyll, A. (2008). *CFD and experimental study of aerodynamic degradation of iced airfoils*. Conference Proceedings presented in Colloquium FLUID DYNAMICS 2008.

Hunsaker, D. (2007). *A numerical blade element approach to estimating propeller flowfields*. Conference Proceedings presented in 45th AIAA Aerospace Sciences Meeting and Exhibit (pp. 374).

Ignatowicz, K., Morency, F. & Beaugendre, H. (2019). *Numerical simulation of ice accretion using Messinger-based approach: effects of surface roughness*. Conference Proceedings presented in CASI Aero 2019-Canadian Aeronautics and Space Institute's AERO 2019 Conference.

Jacob, J. (2006). *Experimental and computational aerodynamic analysis of ice fragments shed from aircraft surfaces*. (Ph.D. thesis).

Janjua, Z. A., Turnbull, B., Hibberd, S. & Choi, K.-S. (2018). Mixed ice accretion on aircraft wings. *Physics of Fluids*, 30(2).

Katz, J., Joseph, Plotkin, A. & Allen. (2001). *Low Speed Aerodynamics*. Cambridge university press. doi: 10.1017/CBO9780511810329.

Láoh, T. (2015). *Numerical simulation of ice accretion on a propeller blade*. (Master's thesis, University of Twente).

Liu, Y., Li, L., Ning, Z. & Hu, H. An Experimental Study on the Transient Ice Accretion Process over the Blade Surfaces of a Rotating UAS Propeller. *SAE Technical report*.

Liu, Y., Li, L., Ning, Z., Tian, W. & Hu, H. (2018). Experimental investigation on the dynamic icing process over a rotating propeller model. *Journal of Propulsion and Power*, 34(4), 933-946.

Lotstedt, P. (1992). Propeller Slip-Stream Model in Subsonic Linearized Potential Flow. *Journal of Aircraft*, 29(6), 1098-1105. doi: 10.2514/3.56865.

Lowe, T. E. *Development of a Microsoft Excel Based Uav Propeller Design and Analysis Tool*. (Ph.D. thesis, Oklahoma State University).

McCormick, B. W. *Aerodynamics, aeronautics, and flight mechanics*. SAGE Publications Sage UK: London, England.

Ozgen, S. & Canıbek, M. (2012). In-flight ice formation simulation on finite wings and air intakes. *The Aeronautical Journal (1968)*, 116(1178), 337-362. doi: 10.1017/S000192400000525X.

Papadakis, M., Yeong, H.-W., Wong, S.-C., Vargas, M. & Potapczuk, M. (2005). Experimental investigation of ice accretion effects on a swept wing. *SAE Technical report*.

Papadakis, M., Yeong, H.-W. & Suares, I. (2007). Simulation of ice shedding from a business jet aircraft. *45th AIAA Aerospace Sciences Meeting and Exhibit*.

Park, M. S. (2015). *Aircraft De-Icing System Using Thermal Conductive Fibers*. (Thesis, Embry-Riddle Aeronautical University Daytona Beach, Florida).

Ramdin, S. (2017). *Prandtl tip loss factor assessed*. (Thesis, Delft University of Technology).

Rausa, A. & Guardone, A. (2021). Multi-physics simulation of in-flight ice shedding. *Journal of Physics: Conference Series*, 1730(1), 012024. doi: 10.1088/1742-6596/1730/1/012024.

Shimoi, K. (2010). *Numerical and experimental investigation of ice shedding*. (Ph.D. thesis, Wichita State University).

Stone, R. H. (2008). Aerodynamic modeling of the wing-propeller interaction for a tail-sitter unmanned air vehicle. *Journal of Aircraft*, 45(1), 198-210.

Suares, I. G. (2005). *Ice particle trajectory simulation*. (Thesis, Wichita State University).

Thomas, S. K., Cassoni, R. P. & MacArthur, C. D. (1996). Aircraft anti-icing and de-icing techniques and modeling. *Journal of aircraft*, 33(5), 841-854.

Tran, P., Brahimi, M., Paraschivoiu, I., Pueyo, A. & Tezok, F. (1995). Ice accretion on aircraft wings with thermodynamic effects. *Journal of Aircraft*, 32(2), 444-446.

Trontin, P., Blanchard, G., Kontogiannis, A. & Villedieu, P. *Description and assessment of the new ONERA 2D icing suite IGLOO2D*. Conference Proceedings presented in 9th AIAA Atmospheric and Space Environments Conference (pp. 3417).

Veldhuis, L. L. M. Propeller wing aerodynamic interference. *24th International Congress of the Aeronautical Sciences*.

Walchner, O. (1937). Aerodynamic Theory Berlin 1935, Verlag Julius Springer. Preis geb. 34 M. *ZAMM - Journal of Applied Mathematics and Mechanics*, 17(6), 371-371. doi: https://doi.org/10.1002/zamm.19370170616.

Waldman, R. M. & Hu, H. (2016). High-speed imaging to quantify transient ice accretion process over an airfoil. *Journal of Aircraft*, 53(2), 369-377.

Witkowski, D. P., Lee, A. K. H. & Sullivan, J. P. (1989). Aerodynamic interaction between propellers and wings. *Journal of Aircraft*, 26(9), 829-836. doi: 10.2514/3.45848.